

ADAPTIVE TRELLIS-CODED MODULATION FOR MOBILE COMMUNICATIONS

by

SIAVASH MASSOUMI ALAMOUTI

B.A.Sc. (EE), University of British Columbia, 1989.

A THESIS SUBMITTED IN PARTIAL FULFILLMENT OF

THE REQUIREMENTS FOR THE DEGREE OF

MASTER OF APPLIED SCIENCE

in

THE FACULTY OF GRADUATE STUDIES

DEPARTMENT OF ELECTRICAL ENGINEERING

We accept this thesis as conforming

to the ~~required~~ standard

| | |
|-------|-------|
| _____ | _____ |
| _____ | _____ |
| _____ | _____ |
| _____ | _____ |

The UNIVERSITY OF BRITISH COLUMBIA

November 1991

© Siavash M. Alamouti, 1991

In presenting this thesis in partial fulfilment of the requirements for an advanced degree at the University of British Columbia, I agree that the Library shall make it freely available for reference and study. I further agree that permission for extensive copying of this thesis for scholarly purposes may be granted by the head of my department or by his or her representatives. It is understood that copying or publication of this thesis for financial gain shall not be allowed without my written permission.

(Signature) _

Department of Electrical Engineering
The University of British Columbia
Vancouver, Canada

Date NOV 22, 1991

Abstract

An adaptive scheme for trellis-coded modulation of MPSK signals called adaptive trellis-coded multiple-phase-shift-keying (ATCMPSK) is proposed for Rayleigh fading channels. The adaptive scheme employs a slightly modified rate $1/2$ convolutional encoder and the corresponding Viterbi decoder to realize a family of codes of different rates which are employed according to channel conditions. During poor channel conditions, trellis-coded QPSK (TCQPSK) together with repetition schemes are employed. As channel conditions improve, higher rate schemes such as trellis-coded 16PSK are used. An interleaving/deinterleaving method suitable for the adaptive scheme is proposed. Theoretical bounds for the error performance and throughput of the proposed adaptive scheme are derived, and are compared against the simulation results. Simulations have been performed to measure the performance of the scheme for different parameters and nonideal conditions. It is shown that ATCMPSK results in considerable improvement in bit-error-rate (BER) performance of MPSK signals. Under ideal conditions, gains in the range of 3 – 20 dB are achieved over conventional fixed rate trellis-coded schemes.

Contents

| | |
|---|----|
| Abstract | ii |
| List of Figures | vi |
| List of Tables | ix |
| Acknowledgement | x |
| Chapter 1 Introduction | 1 |
| Chapter 2 Review of Trellis-Coded Modulation | 5 |
| Chapter 3 Pragmatic TCM | 9 |
| Chapter 4 Adaptive Trellis-Coded MPSK (ATCMPSK) | 12 |
| Section 1 Fading Channel Model | 12 |
| Topic 1 The Gaussian Metric | 14 |
| Section 2 Description of the Overall System Model | 16 |
| Topic 1 Interleaving/Deinterleaving | 20 |
| Chapter 5 Performance of Pragmatic TCM | 23 |
| Section 1 Theoretical Bound on the BER in AWGN | 23 |
| Topic 1 T(D) and the Error-State Diagram | 25 |
| Topic 2 Simplified Error-State Diagram | 29 |
| Section 2 BER Performances of Various Pragmatic TCM Schemes in AWGN | 29 |
| Topic 1 Rate 1/2 TCQPSK in AWGN | 30 |
| Topic 2 Rate 2/3 TC8PSK in AWGN | 34 |

| | | |
|-----------|--|----|
| Topic 3 | Rate 3/4 TC16PSK in AWGN | 38 |
| Section 3 | BER Performance of Pragmatic TCM Schemes in the Rayleigh Fading Channel | 44 |
| Chapter 6 | Performance of ATCMPSK in the Rayleigh Fading Channel | 51 |
| Section 1 | Bound on the BER performance of ATCMPSK in the Rayleigh Fading Channel | 51 |
| Section 2 | Throughput of ATCMPSK | 56 |
| Chapter 7 | Description of Computer Simulations | 60 |
| Section 1 | The AWGN Channel | 60 |
| Section 2 | The Rayleigh Fading Channel | 61 |
| Topic 1 | Jakes' Model of Rayleigh Fading (Land-Mobile) | 62 |
| Section 3 | Simulation of the codulator/decodulator | 64 |
| Section 4 | Performance Evaluation Results | 66 |
| Topic 1 | Effect of Error Thresholds on the BER Performance and Throughput | 66 |
| Topic 2 | Effect of Finite Interleaving | 69 |
| Topic 3 | Comparison of ATCMPSK with Nonadaptive TCM Schemes | 70 |
| Topic 4 | Effect of Vehicle Speed or $B_d T_s$ Product | 75 |
| Topic 5 | Effect of Feedback Delay and Adaptation Interval | 78 |

| | | |
|---------------------|--|-------------|
| Chapter 8 | Conclusions and Recommendations for Future Research | . 82 |
| Bibliography | | . 85 |
| Appendix A | The Gaussian Metric | . 87 |
| Appendix B | Comparison of Double-Gray-Coded Mapping and Sectorized-Gray-Coded Mapping | . 91 |
| Section 1 | Comparison in AWGN | . 91 |
| Section 2 | Comparison in Rayleigh Fading Channel | . 93 |
| Appendix C | Confidence Interval for Simulation Results | . 96 |

List of Figures

| | | |
|-----------|--|----|
| Figure 1 | Trellis encoder and MPSK mapper structure. | 6 |
| Figure 2 | Mapping by set partitioning of the 8PSK signal space. . . | 6 |
| Figure 3 | A rate 2/3 trellis-coded scheme and its set partitioned 8PSK signal space. | 8 |
| Figure 4 | Pragmatic encoder and its trellis structure for $K=3$ | 9 |
| Figure 5 | Double-Gray-coded mapping for 16PSK. | 11 |
| Figure 6 | Comparison between the Euclidean distance and the Gaussian distance. | 15 |
| Figure 7 | Simplified block diagram of ATCMPSK. | 16 |
| Figure 8 | Interleaver Structure for ATCMPSK. | 21 |
| Figure 9 | The structure of the deinterleaver for ATCMPSK. | 22 |
| Figure 10 | The general structure of the error-state diagram for pragmatic codes ($K=3$). | 28 |
| Figure 11 | Trellis diagram and the signal space for rate 1/2 TCQPSK. | 31 |
| Figure 12 | BER Performance of rate 1/2 TCQPSK code in AWGN. . . | 34 |
| Figure 13 | Trellis structure, and the signal space for the rate 2/3 pragmatic code. | 35 |
| Figure 14 | Parallel branches in the trellis for the rate 2/3 code. | 37 |
| Figure 15 | BER performance of the rate 2/3 TC8PSK code in AWGN. | 38 |

| | | |
|-----------|---|----|
| Figure 16 | Trellis structure and signal space for rate 3/4 pragmatic code with double-Gray-coded mapping. | 39 |
| Figure 17 | Parallel branches in the trellis diagram of rate 3/4 pragmatic code. | 42 |
| Figure 18 | BER performance of rate 3/4 TC16PSK code in AWGN. | 44 |
| Figure 19 | BER performance of ideally interleaved trellis-coded MPSK in Rayleigh fading. | 49 |
| Figure 20 | Theoretical and simulation curves for the BER performance of ATCMPSK under Rayleigh Fading. | 56 |
| Figure 21 | Information throughput of ATCMPSK—simulation and theory. | 59 |
| Figure 22 | Block diagram of the baseband land-mobile fading simulator. | 64 |
| Figure 23 | Adaptation thresholds for ATCMPSK. | 66 |
| Figure 24 | BER performance of ATCMPSK with different error roofs. | 67 |
| Figure 25 | Throughput of ATCMPSK for different error roofs. | 68 |
| Figure 26 | Effect of finite interleaving on BER performance of ATCMPSK. | 70 |
| Figure 27 | BER curves for ATCMPSK and fixed rate TCQPSK, with superimposed curve of the throughput performance of ATCMPSK. | 71 |

| | | |
|-----------|--|----|
| Figure 28 | BER curves for ATCMPSK and fixed rate TC8PSK, with superimposed curve of the throughput performance of ATCMPSK. | 74 |
| Figure 29 | Effect of vehicle speed on the BER performance of ATCMPSK with delayless feedback. | 76 |
| Figure 30 | Effect of vehicle speed on the BER performance of ATCMPSK, feedback delay = 1 symbol duration. | 77 |
| Figure 31 | Effect of vehicle speed on the BER performance of ATCMPSK, feedback delay = 3 symbol durations. | 78 |
| Figure 32 | Effect of feedback delay on the BER performance of ATCMPSK. | 79 |
| Figure 33 | Effect of nonideal adaptation on the BER performance of ATCMPSK. | 80 |
| Figure 34 | Correlator receiver for maximum likelihood detection. | 87 |
| Figure 35 | Comparison of signals on the parallel branches of the trellis diagram for double-Gray-coded and sectorized-Gray-coded mappings. | 91 |
| Figure 36 | Comparison of trellis error and probability of error due to parallel transitions for TC16PSK in AWGN with sectorized-Gray-coded and double-Gray-coded mapping. | 93 |
| Figure 37 | BER performance of double-Gray-coded TC16PSK. | 95 |

List of Tables

| | | |
|---------|--|----|
| Table 1 | Error-weight profiles for the rate 2/3 pragmatic code. . . . | 36 |
| Table 2 | Error weight profiles for rate 3/4 pragmatic code with double-Gray-coded mapping. | 40 |
| Table 3 | Proportion of errors for the various schemes used in ATCMPSK. Error roof = 0.01, interleaving size = 32*16, SNR=24 dB. | 73 |
| Table 4 | Error weight profile for the rate 3/4 TC16PSK pragmatic code with sectorized-Gray-coded mapping. | 92 |

Acknowledgement

I would like to thank my long time companion Gaylynn Noonan for her moral support and constant encouragement. I send my regards to my mother Atiye Shaeri, and my father Ahmad M. Alamouti for their love, nurturing and support. I am indebted to my supervisor, Dr. Samir Kallel, for his constant guidance and his indispensable role in the successful completion of this thesis. I express my gratitude to Dr. A. D. Moore, and Dr. Cyril Leung for having played a major part in my decision to enter the most fascinating field of communications. I extend my appreciation to B.C. Science Council for their financial support, to Dr. Norman Toms at MPR for his encouragement as the industrial supervisor of this project , and to MDI and MPR for their support as cooperating companies. I would also like to thank my good friends and fellow students in the communications group of the Electrical Engineering department of UBC for their dedication to providing a friendly and cooperative environment for research. Finally, I would like to thank Dr. Takis Mathiopolous for his careful examination of this thesis.

Chapter 1

Introduction

The rapid progression of mobile communication technology from analog to digital has made available a new variety of services. Mobile systems are no longer dedicated solely to speech transmission [1]. Reliable transmission of data, and integrated services have gained a lot of importance in today's era of information. There is a great demand for mobility, reliability, and speed in transmission of information. Frequency spectrum is, however, a limited resource. Therefore, in order to maximize the services offered through mobile communications, frequency spectrum must be used efficiently. Spectrally efficient linear modulation schemes increase the effective rate of transmission of information without any added spectrum. One widely used, linear modulation scheme is *multiple-phase-shift-keying* or MPSK. MPSK schemes are spectrally efficient, simple to implement, and have relatively good bit-error-rate (BER) performance. But, as there is usually a trade off between power and spectral efficiency, MPSK schemes are less power efficient.

Power efficiency is a major issue in mobile communications. To keep the size of the mobile units small, the power consumption must be minimized. To minimize the required power to achieve a certain BER, error control techniques can be applied. The combination of convolutional encoding and Viterbi decoding is a widely used forward-error-correction (FEC) technique. Furthermore, considerable gains can be attained through combining MPSK modulation and coding through trellis-coded modulation (TCM). TCM was first explored by Ungerboeck [2] who showed that, in the AWGN channel, gains of up to 6 dB were attainable without any bandwidth expansion, and that most of the coding

gain could be obtained by doubling the size of the signal space. For example, using a rate $2/3$ convolutional code together with an 8PSK signalling scheme, 3–4 dB of gain can be obtained as compared to uncoded QPSK—although both schemes have the same information rate of 2 bits per symbol duration.

Although conventional TCM schemes offer appreciable coding gains in AWGN, their performance suffers greatly in the Rayleigh fading environment. The time varying nature of the channel imposes a great constraint on the TCM scheme employed to combat the effect of fading. MPSK schemes with more than four signals in their constellation have, for most applications, unacceptable BER performance, while lower level MPSK schemes such as BPSK greatly sacrifice the throughput. Moreover, it has been shown that a lot can be gained—in terms of BER and throughput performance—by variable rate transmission of information on fading channels [3]. These facts justify the implementation of an adaptive scheme using trellis-coded MPSK signals.

The proposed adaptive scheme is based on a simple pragmatic encoder/modulator [4]. The principal advantage of the scheme is that the same encoder/decoder can be used for a wide variety of trellis codes. The system can generate different trellis-coded signals using the same rate $1/2$ convolutional encoder. The adaptive nature of the scheme allows for lowering the coding rate while keeping the same symbol transmission rate during deep fades. The coding/modulation (codulation) rate is changed according to channel conditions determined by the signal level detected at the receiver. If the signal level drops below a predetermined threshold, then the encoder is informed through a feedback channel, and the codulation rate is changed accordingly. If channel conditions become extremely bad, repetition codes together with trellis-coded QPSK (TCQPSK) are applied.

This thesis has been organized in the following manner:

Chapter 2 is a brief review of trellis-coded modulation. In Chapter 3, the pragmatic approach to trellis-coded modulation is discussed, and the fact that is suitable for use in adaptive systems is explained. In Chapter 4, we introduce the adaptive scheme and the various elements needed for its design. A suitable approach to interleaving/deinterleaving for the adaptive scheme is also introduced in this Chapter. Chapter 5 has been dedicated to a detailed analysis of the error performance of the pragmatic schemes employed in the adaptive system both in AWGN and Rayleigh fading channels. All the theoretical analysis of error performance are based on the classical transfer function approach. In Chapter 6, theoretical analysis for the bit-error probability and the throughput of ATCMPSK under ideal conditions are carried out. Finally, in Chapter 7, the details of simulation programs are explained, and the results of simulations are reported. Simulations have been run for various parameters to take into account the effects of nonideal conditions.

The contributions of this thesis to digital communications theory are as follows:

- Derivation of relatively tight theoretical upper bounds for the performance of some pragmatic TCM schemes in AWGN, and Rayleigh fading channels.
- Introduction of a new signal mapping scheme suitable for the adaptive scheme; and, in fact, all pragmatic trellis-coded MPSK schemes using a signal constellation with 16 or more signals.
- Design and investigation of an adaptive system used for the purpose of communications over time varying channels, specifically Rayleigh fading channels.
- Derivation of a theoretical bound on the BER, and exact expressions for the throughput performance of the proposed ATCMPSK scheme, under ideal conditions.

- Simulation of the ATCMPSK scheme, taking into account many parameters such as vehicle speed, feedback delay, adaptation interval, and adaptation thresholds.

Chapter 2

Review of Trellis-Coded Modulation

The fundamental idea behind the design of any TCM scheme is combining the functions of coding and modulation. Before this revolutionary idea was introduced by Ungerboeck [2], coding and modulation were conceived as two separate functions. The separation of these two functions led to an unrecoverable loss of information due to hard quantization, and nonideal code optimization. Traditionally, code optimization was carried out independently from the signal geometry of the modulation scheme. All that was considered was the Hamming distance between binary sequences. Generally, the Hamming distance between binary representations of two signals does not translate to their distance in the signal space. Therefore, one can say that Hamming distance is often not a true measure of similarity between signal representation of two symbols. On the other hand, the geometric distance between the signals or their *Euclidean distance* (ED) is an exact measure.

Ungerboeck [2], [5] showed that using ED as the metric in systems employing convolutional coding and Viterbi decoding, and designing codes to achieve maximum ED between all possible sequences of channel signals leads to significant coding gains without any sacrifice in bandwidth or the effective information rate. As opposed to conventional FEC techniques, where the redundancy is added to information bits, the required redundancy for error correction is obtained by expanding the size of the signal space. In fact, it was shown [2] that nearly all the possible gain in performance is achieved by doubling the size of the signal space. This led to the design of rate $n/n+1$ codes with

signal spaces of size $M=2^{n+1}$. Figure 1 shows the trellis encoder with an M level mapper.

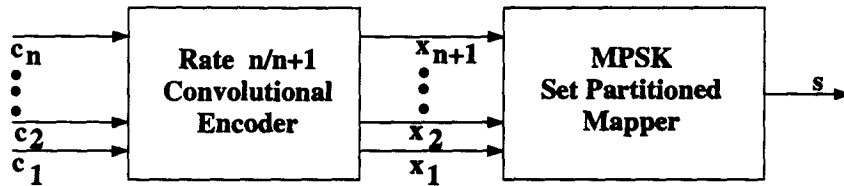


Figure 1 Trellis encoder and MPSK mapper structure.

The optimum signal mapping is based on partitioning the signal space into subsets with increasing minimum distances, and assigning bits to transitions to each sub-partition. The example for 8PSK is shown in Figure 2. It is interesting to note that for MPSK we can achieve a set-partitioned signal space by consecutive binary numbering of the signals in the signal space starting from a reference point.

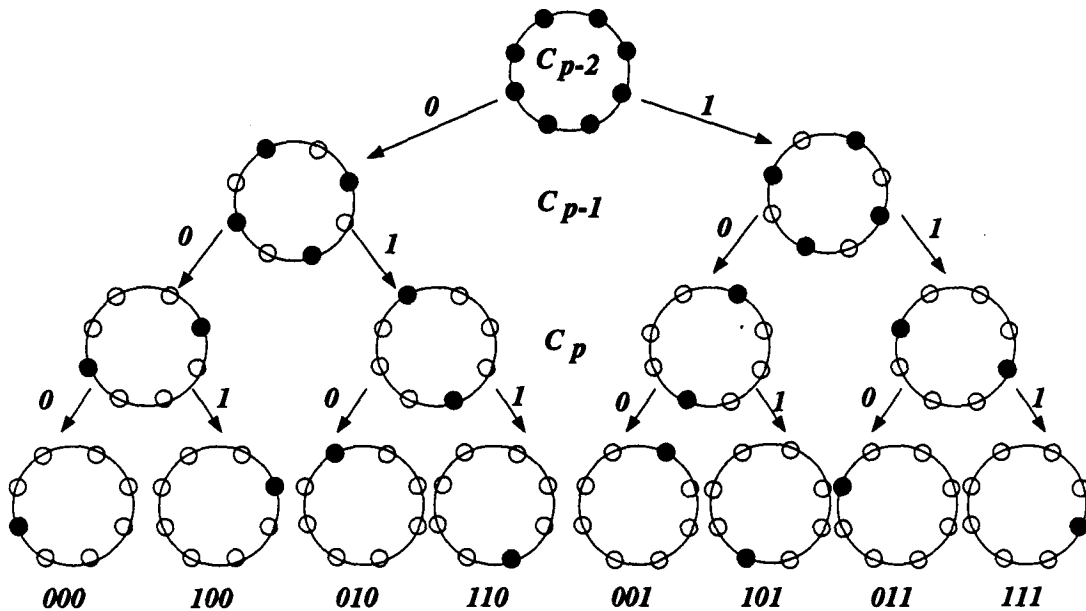


Figure 2 Mapping by set partitioning of the 8PSK signal space.

The design of a trellis-coded scheme is aimed primarily at maximizing *Euclidean free distance* d_{free} defined as:

$$\begin{aligned} d_{free}^2 &= \min_L [d^2(X_L, X'_L)] \\ &= \min_L \left[\sum_{n=1}^L d^2(x_n, x'_n) \right]. \end{aligned} \quad (2.1)$$

where $X_L = (x_1, x_2, \dots, x_L)$, $X'_L = (x'_1, x'_2, \dots, x'_L)$ are two sequences of encoded symbols of length L , and $d(x_n, x'_n)$ is the ED between the two signals.

The first step in designing an optimum code is to choose a suitable trellis structure. The choice of the trellis structure depends mainly on the constraint length of the code, since it determines the overall shape of the trellis and the number of states. Codes with higher constraint length have superior performance; however, they are more costly to implement both in terms of hardware and design effort.

Having chosen the suitable trellis structure, signals from the MPSK signal space should be assigned to state transitions on the trellis so that d_{free} is maximized. For codes of large constraint length, this is done using a computer algorithm that assigns signal to the transitions and measures d_{free} until it achieves the optimum configuration. For smaller constraint lengths, a few rules of thumb can ensure an optimum design for the chosen trellis structure.

1. Having partitioned the signal space into subsets with increasing Euclidean distances, assign to parallel transitions signals in the subset of the signal space C_p (see Figure 2) whose members have as many signals as the number of parallel transitions, and maximum distance between all pairs of signals.
2. To transitions originating from the same state or joining into the same state assign the signals in the subset preceding C_p in the partition process.

3. Make sure that all states, and the signals in the signal space are on equal footing.

Figure 3 shows an example of a rate 2/3 trellis-coded 8PSK scheme which has been designed using the above guidelines. In this example, there are two parallel branches in each transition.

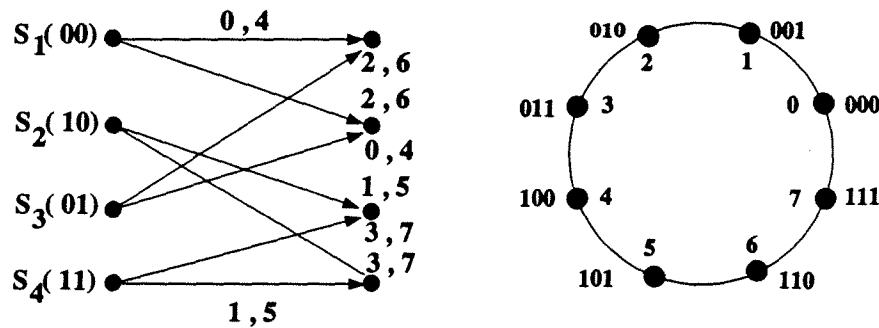


Figure 3 A rate 2/3 trellis-coded scheme and its set partitioned 8PSK signal space.

Note that signals on the parallel transitions have been assigned in such a way as to maximize the distance between them which for the special case of 8PSK this corresponds to antipodal signals.

One major drawback of Ungerboeck's family of trellis codes is that each signal configuration requires a different encoder/decoder—since optimized TCM schemes of different rates have different code structures. The use of these codes in adaptive systems would therefore be costly. A less expensive and more pragmatic alternative is to use the set of pragmatic trellis codes.

Chapter 3

Pragmatic TCM

Recently, Viterbi *et al.* [4] proposed a pragmatic approach to trellis-coded modulation which is based on the realization of rate $n/n+1$ trellis-coded schemes using a single rate $1/2$ encoder/decoder, in conjunction with an MPSK signal mapper where $M=2^{n+1}$. The name pragmatic refers to code implementation employing the widely used, best known rate $1/2$ convolutional encoder, and the corresponding Viterbi decoder.

Figure 4 shows the pragmatic encoder, and the corresponding trellis diagram for the “good”¹ convolutional code of constraint length $K=3$.

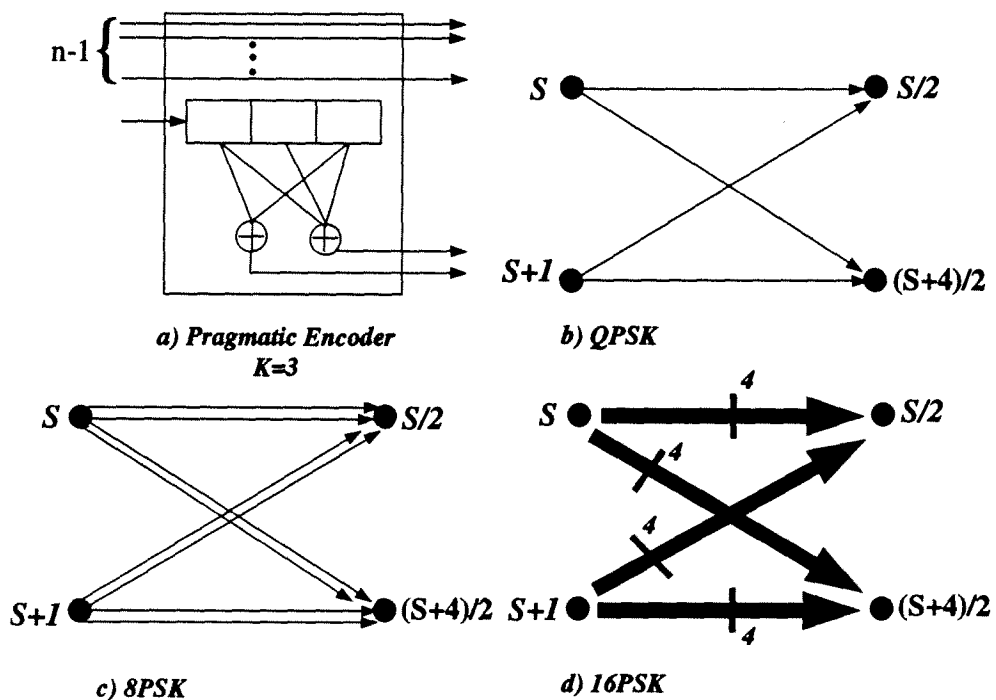


Figure 4 Pragmatic encoder and its trellis structure for $K=3$.

¹ Good codes refer to codes optimized for minimum Hamming distance.

Information bits are fed serially into the encoder. One out of every n bits is sent into the rate $1/2$ encoder, and the remaining $n-1$ bits pass directly through without being encoded. In this manner, trellis codes of various rate are generated. The number of uncoded bits determine the rate of the code. Different rate codes differ only in the number of parallel transitions in their respective trellis diagrams. The trellis diagram for rate $1/2$ TCQPSK does not have any parallel branches. However, rate $2/3$ TC8PSK has 2 parallel branches in each state transition. In general, rate $n/n+1$ TCMPSK pragmatic trellis codes have $M/4$ parallel branches in each state transition.

The mapping scheme suggested in [4] can be called *sectorized-Gray-coded mapping*, and it works as follows: the $n+1$ bits at the output of the encoder are used to select a signal in the signal space. The two least significant bits, which are the output of the rate $1/2$ encoder, select one out of four signals according to Gray code. The remaining $n-1$ bits choose a sector in the signal space lexicographically, as shown in Figure 5 for the case of 16PSK. Note that equivalent signals in different sectors (signals with identical two least significant bits) belong to parallel branches of the same state transition.

In this thesis, we suggest a different mapping scheme which we choose to call *double-Gray-coded mapping*. As for sectorized-Gray-coded mapping, the two least significant bits corresponding to the output of the rate $1/2$ encoder select one out of four signals according to Gray code. The remaining $n-1$ bits choose a sector in the signal space again according to Gray code, as depicted in Figure 5 for 16PSK signalling scheme. The first two bits of the encoded symbol determine the sector to which the signal belongs. Note that both mapping schemes result in the same signal space for constellations with less than 16 signals.

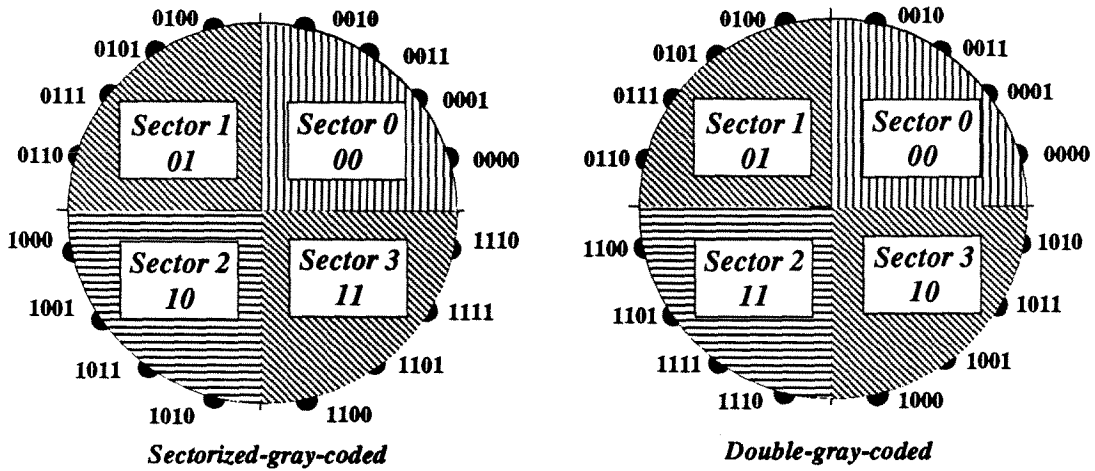


Figure 5 Double-Gray-coded mapping for 16PSK.

The obvious advantage of the double-Gray-coded mapping scheme for 16PSK is that signals belonging to parallel branches of neighbouring sectors differ in one bit as compared to 2 bits for sectorized-Gray-coded mapping. This will definitely improve the error performance of the code since most of the errors happen in neighbouring sectors. The BER performance of the trellis-coded 16PSK signals using the two different mapping schemes are compared in Appendix B. The mapping scheme employed throughout this research is double-Gray-coded MPSK, unless otherwise stated.

It is shown in [4] that, for all practical purposes, the asymptotic coding gains (ACG) of the pragmatic codes are almost the same as Ungerboeck's codes. The amount of sub-optimality introduced is negligible for MPSK signals. The code, however, is much simpler to implement, and the same decoder can be used for different modulation rates.

Chapter 4

Adaptive Trellis-Coded MPSK (ATCMPSK)

Although pragmatic trellis codes perform nicely in the AWGN environment, they are not nearly as good in the fading environment. The major reason for this degradation in performance is the presence of parallel transitions in their state diagram which give rise to single signal error events. Therefore, in order to keep the BER lower than a certain level, lower rate pragmatic codes must be used—since going into higher rates will have catastrophic results during deep fades. But channel conditions are not always bad. A fixed low rate code will sacrifice the throughput even during good channel conditions. Therefore, a system is needed that can take advantage of periods of good channel conditions to transmit at a higher rate, and can lower its rate during deep fades.

Adaptive schemes have shown to be an effective method for combating the time varying nature of the distortion in the fading channel. A series of published papers report considerable gains by adapting certain parameters in the transmitter according to channel conditions—from symbol duration and power to transmission rate [6], [7], [3].

4.1 Fading Channel Model

The model for the fading channel used in this study is that presented by Jakes in [8]. It is assumed that the received field at the mobile unit is made up of a number \hat{N} of waves arriving with different amplitudes and angles of incidence in a random fashion. If the transmitted signal is vertically polarized, the received signal can be expressed as:

$$E_z = I(t) \cos(2\pi f_c t) - Q(t) \sin(2\pi f_c t) \quad (4.1)$$

where

$$\begin{aligned}
 I(t) &= E_0 \sum_{n=1}^{\hat{N}} C_n \cos(2\pi f_n t + \phi_n) \\
 Q(t) &= E_0 \sum_{n=1}^{\hat{N}} C_n \sin(2\pi f_n t + \phi_n)
 \end{aligned}
 \tag{4.2}$$

are Gaussian processes. At any instant of time, the samples of these processes are uncorrelated Gaussian random variables with zero mean, and variance $b_0 = E_0^2/2$. The envelope of the faded signal

$$\alpha = \sqrt{\|I(t)\|^2 + \|Q(t)\|^2}
 \tag{4.3}$$

is then Rayleigh distributed with probability density function

$$f(\alpha) = \frac{\alpha}{b_0} \exp\left(-\frac{\alpha^2}{2b_0}\right) \quad \alpha \geq 0,
 \tag{4.4}$$

where $\|\cdot\|$ stands for magnitude. Throughout this thesis we shall assume that $b_0=0.5$ so that $E_0^2 = 1$. Or equivalently:

$$f(\alpha) = 2\alpha \exp(-\alpha^2) \quad \alpha \geq 0.
 \tag{4.5}$$

The phase of the fading signal is uniformly distributed. We will assume that the effect of phase on the received signal is fully compensated for by the receiver. This can be done in practice by pilot tone insertion and calibration [9], [10], or tracking the phase by a phase locked loop [11]. We should keep in mind, however, that in a fading environment, the exact tracking of the phase is extremely difficult. In fact, differential detection seems to be one of the only viable solutions for this problem [12]. Simon and Divsalar [13] have devised a differential detection scheme for MPSK signals called *multiple-symbol differential detection*, which is based on maximum-likelihood sequence

estimation. Their idea can be applied to differential detection of TCMPSK signals. If a more realistic model is desired, the effect of phase error can usually be modelled by a Gaussian random variable [14].

Considering only the effect of fading on the amplitude of the transmitted signal is the same as multiplying the in-phase and quadrature components of the baseband signal by the time varying fading amplitude $\alpha(t)$.

4.1.1 The Gaussian Metric

Since the transmitted signal is attenuated by the fading component α , the square of the Euclidean distance is no longer an accurate, or optimum measure of the similarity between the received signal and branch signals in the trellis diagram and hence not an optimum metric. Figure 6 illustrates this concept geometrically.

S_1, S_2 are signals in the signal-space, R_f is the faded signal at the receiver, and R_g would be the received vector if fade was not present (AWGN channel). Distance d is the ED between R_f, S_1 . This ED is distorted by fading. However, N , the length of the AWGN vector, and the distance between R_f and the faded transmitted signal S'_1 , is exactly the same as the distance between R_g, S_1 (the case of AWGN channel). Therefore, if the right decision is made, and N^2 is chosen as the metric, one should expect the same performance as in the AWGN channel. Of course, this is not the case since the attenuation reduces the signal energy which in turn increases the probability of error, and causes an overall degradation in performance.

In conclusion, using optimum decision rules for matched filter detection to minimize the probability of error, one would find that the square of the distance between the faded

transmitted signal and the received signal is the optimum metric. This metric is often called the *Gaussian metric* [15].

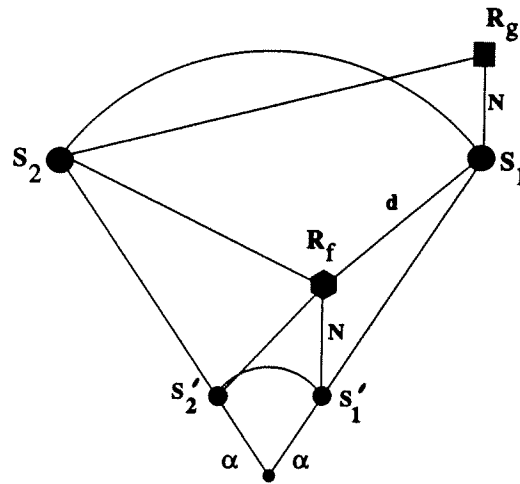


Figure 6 Comparison between the Euclidean distance and the Gaussian distance.

Assume that a sequence of signals $X = (x_1, x_2, \dots, x_L)$ is transmitted, signals $Y = (y_1, y_2, \dots, y_L)$ are received, and the corresponding fading amplitudes are :

$$A = (\alpha_1, \alpha_2, \dots, \alpha_L) \quad (4.6)$$

then $y_i = \alpha_i x_i + n_i$ for $1 \leq i \leq L$, where

$$n_i \sim N\left(0, \frac{N_0}{2}\right) \quad (4.7)$$

is a sample of AWGN, and $\frac{N_0}{2}$ is its power spectral density. The metric associated with

the i th symbol can be written as:

$$m_i = |y_i - \alpha_i x_i|^2. \quad (4.8)$$

For a mathematical proof of the optimality of Gaussian metric refer to Appendix A.

4.2 Description of the Overall System Model

The adaptive scheme presented in this thesis (ATCMPSK) is conceptually simple to implement. We call it *adaptive trellis-coded multiple-phase-shift-keying* to accentuate the combined coding/modulation (codulation) aspect of the scheme. A simplified block diagram of the proposed ATCMPSK scheme is shown in Figure 7.

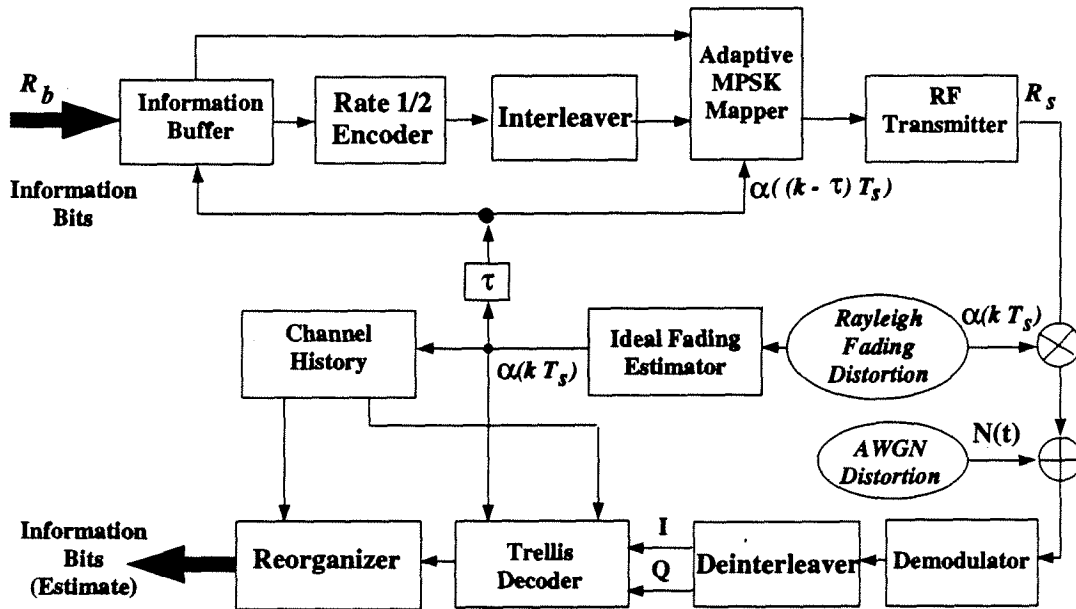


Figure 7 Simplified block diagram of ATCMPSK.

Information bits enter the information buffer at rate R_b bits/sec. The buffer is needed since, as it will be discussed shortly, the effective rate of information is a function of the conditions in the time varying channel and is hence not fixed, but the symbol transmission

rate $R_s = \frac{1}{T_s}$ is constant. In order to choose the suitable scheme for transmission we need channel state information (CSI) which in our model is the amplitude of fading $\alpha(kT_s)$ at the start of the transmission and is supplied by the ideal fading estimator to the transmitter so that it can adjust its rate according to channel conditions, and to the receiver for the purpose of decoding. As shown in the block diagram, we assume that the receiver has ideal CSI, while, in general, the transmitter receives a delayed version of CSI which in our model we assume is an integer multiple of symbol duration, and we have hence denoted it by $\alpha((k - \tau)T_s)$. The assumption that the receiver has ideal CSI without any delay is reasonable since usually CSI is obtained by methods such as pilot tone insertion and extraction [10], [9] which determine an estimate of the channel at the receiver side.

The transmitter decides what scheme should be used at the start of every transmission according to a set of given thresholds that have been chosen to keep the BER below a certain level. We assume that there are five possible schemes to choose from:

1. Rate 1/2 TCQPSK with 3 repetitions
2. Rate 1/2 TCQPSK with 2 repetitions
3. Rate 1/2 TCQPSK
4. Rate 2/3 TC8PSK
5. Rate 3/4 TC16PSK.

Rate 1/2 TCQPSK with 3 repetitions is used during the worst, and rate 3/4 TC16PSK during the best channel conditions. Since there are five different codes employed by the ATCMPSK under study, we have four adaptation thresholds. Assume that these adaptation thresholds are $\mu_1, \mu_2, \mu_3, \mu_4$ ². The transmitter looks at the value of the

² The way in which these thresholds are chosen is discussed in Section 7.4.1

immediate SNR defined as:

$$SNR_i = \alpha_i^2 \frac{E_s}{N_0}, \quad (4.9)$$

and determines the suitable modulation scheme. If $0 \leq SNR_i \leq \mu_1$ rate 1/2 TCQPSK with 3 repetitions is employed. Otherwise, if $\mu_1 \leq SNR_i \leq \mu_2$ rate 1/2 TCQPSK with two repetitions is chosen as the modulation scheme suitable for transmission, and so on. One could extend the idea to systems which employ more diverse schemes to attain larger throughput during very good channel conditions, and superior error performance during very poor channel conditions at the expense of lower throughput of information. The main trade off in such schemes is between performance and implementation cost.

Going back to the block diagram, information bits are fed into a rate 1/2 convolutional encoder, passed to the interleaver, and combined with the appropriate number of information bits (according to CSI) to form the adaptively encoded channel symbol³. The encoded channel symbol is then mapped into a baseband signal according to double-Gray-coded mapping discussed in Chapter 2. The baseband signals are modulated by the carrier, and sent over the channel. A more realistic model would include a digital pulse shaper to combat ISI, and pilot tone insertion to help estimate the value of fading.

The only sources of distortion are assumed to be the AWGN and the envelope attenuation due to fading. The demodulator recovers the distorted in-phase and quadrature (I/Q) components of the baseband signal which are then passed to the deinterleaver which reestablishes the correct order of rate 1/2 encoded symbols. However, as it will be discussed shortly, the order in which appended information bits are transmitted is not restored until the decoding function has been performed. Finally, the decoder, which is

³ We shall shortly discuss the interleaving/deinterleaving function in detail.

a slightly modified rate 1/2 Viterbi decoder, decodes the received sequence of symbols, and delivers them to the reorganizer which restores the original order of the information sequence. The Viterbi decoder is capable of constructing parallel branches in its trellis diagram. Changing to a different modulation scheme is then equivalent to changing the number of parallel branches in each state transition. The output of the reorganizer is an estimate of the information bits produced by the source.

Note that the same encoder/decoder is used for different modulation rates. The mapping scheme can either be realized by simple table-look-up methods, or, due to its regular structure, by a simple algorithm.

The MPSK mapper/transmitter can accommodate repetition codes. The concept of repetition codes is based on repeating the information to lower the BER [16]. During bad channel conditions, the signal representation of the encoded symbol is transmitted R times. This has the same effect as multiplying the signal energy by R , and may also help the signal recover from a relatively short fade by increasing signal's duration. Of course, the cost of improvement in BER performance is a reduction in throughput.

To accommodate repetition codes, the decoder should allow for multiple signals on the same branch. That is, the metrics for the received repeated signals are added up for the calculation of the final metric. For example, if S_i was transmitted R times and $R_i = (r_{i1}, r_{i2}, \dots, r_{iR})$ is received, then the branch metric for the transition corresponding to branch signal B_k ($1 \leq k \leq M$) is:

$$m_{ik} = \sum_{j=1}^R |r_{ij} - B_k|^2 \quad (4.10)$$

4.2.1 Interleaving/Deinterleaving

Interleaving is traditionally performed to convert channels with memory to memoryless channels. It has the same effect as removing the correlation between the samples of Rayleigh fading, and hence combats the disastrous effect of deep fades on the reconstruction procedure in the trellis, during decoding [17]. Conventional interleaving and deinterleaving consists of storing encoded symbols into a matrix in successive rows, and transmitting the symbols in successive columns thus removing the correlation between the symbols for the adjacent branches of the trellis. The interleaving matrix Z_i has size $s \times d$ where d is called the *interleaving depth* and s the *interleaving span*. The deinterleaver performs the opposite operation. It stores the received symbols in successive columns, and delivers them to the decoder in successive rows, and hence restores the original order of the transmitted symbols.

Conventional interleaving/deinterleaving, however, is not appropriate for ATCMPSK. Storing the encoded symbols in a matrix introduces an unavoidable delay; therefore, by the time an interleaved symbol is sent for transmission, channel conditions may have changed, and the encoded signal may no longer have the suitable scheme for transmission. We should therefore devise a new interleaving method. Figure 8 shows the structure of the interleaver for the proposed scheme.

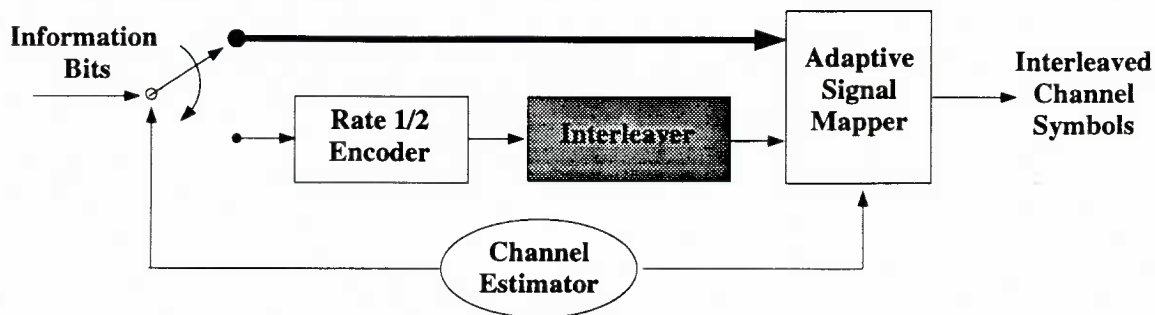


Figure 8 Interleaver Structure for ATCMPSK.

Information bits are passed to the encoder, and the encoded symbols are then delivered to the interleaver where they are stored in a serial fashion in successive rows of the interleaving matrix Z_i until it is filled. The commutator receives CSI from the channel estimator. If channel conditions allow for higher level modulation schemes (TC8PSK, TC16PSK), the commutator will redirect the information bit flow to the adaptive mapper, which will take in the appropriate number of information bit(s) (1 for 8PSK, or 2 for TC16PSK) together with rate 1/2 encoded symbols which are delivered from the interleaver in successive columns, to form the channel symbol.

If channel conditions dictate the use of TCQPSK, the rate 1/2 encoded symbol in the interleaving matrix will be mapped into a QPSK signal (no uncoded bits). Should channel conditions require R repetitions, the mapped QPSK signal is repeated R times. This procedure is repeated, symbol by symbol, until the interleaved symbols are exhausted.

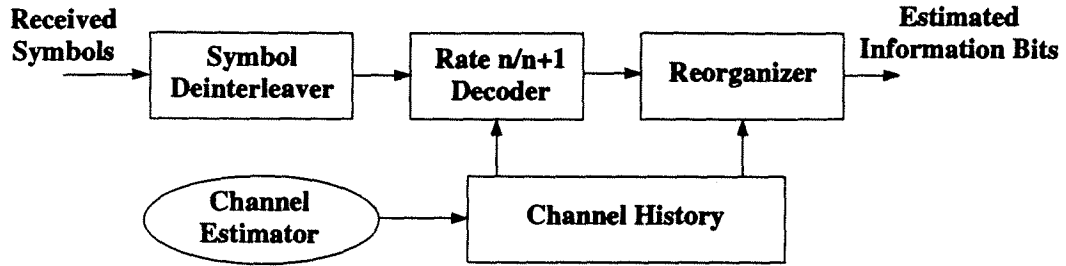


Figure 9 The structure of the deinterleaver for ATCMPSK.

The deinterleaving function is depicted in Figure 9. Received symbols are stored in the successive columns of the deinterleaving matrix Z_d , and are then delivered in successive rows to the Viterbi decoder. By this time, the original order of the rate 1/2 encoded symbols has been restored, but the appended bits are out of order, and cannot be delivered until the whole sequence of symbols (of length equal to the interleaving size) is decoded. The order of the sequence of information bits is then restored by the reorganizer which has the knowledge of the past history of received symbols. The channel history has been stored in an array of the same size as the interleaving/deinterleaving matrix and is shared by the decoder and the reorganizer. The interleaving size is a design specification that is very much application dependent. The most important factor is perhaps the allowable delay due to interleaving/deinterleaving/reorganizing of information symbols. Based on the maximum allowable delay one can choose the interleaving size to keep the delay below the maximum allowable value.

In order to analyze the performance of the ATCMPSK scheme, we need to evaluate the performance of various schemes used to construct it. In the next two chapters we will analyze the BER performance of the pragmatic trellis codes used in ATCMPSK.

Chapter 5

Performance of Pragmatic TCM

5.1 Theoretical Bound on the BER in AWGN

A bound for the BER performance of TCM schemes can be found by applying the idea of the generating function as in the case of linear codes [18]. We will follow the same method as in [19] for performance evaluation of trellis codes. The steps involved are as follows:

- Determine the trellis structure, and finite state diagram of the code.
- Break the finite state diagram at one state so that transitions start from a certain state and end at that same state (commonly the all zero state.) This is called the *error-state diagram*.
- Using the trellis diagram of the code, and ED between symbols on the branches of the trellis diagram determine the branch gains of the error-state diagram.
- From the error-state diagram derive the transfer function $T(D, I)$.
- From $T(D, I)$ find the bit-error probability.

Let $X_L = (x_1, x_2, \dots, x_L)$, $X'_L = (x'_1, x'_2, \dots, x'_L)$ be two sequences of encoded symbols with length L , and $P(X_L \rightarrow X'_L)$ be the pairwise error probability; that is, the probability of choosing X'_L given X_L was transmitted. The union bound on the probability of an error event can then be expressed as [19]:

$$P(e) \leq \sum_{L=1}^{\infty} \sum_{X'_L} \sum_{X_L \neq X'_L} P(X_L) P(X_L \rightarrow X'_L). \quad (5.1)$$

Assuming maximum-likelihood detection [18, p. 247]:

$$P(X_L \rightarrow X'_L) = Q\left(d_M(X_L, X'_L) \sqrt{\frac{E_s}{2N_0}}\right) \quad (5.2)$$

where

$$d_M^2(X_L, X'_L) = \|f_M(X_L) - f_M(X'_L)\|^2 = \sum_{n=1}^L \|f_M(x_n) - f_M(x'_n)\|^2, \quad (5.3)$$

where $\|\cdot\|$ represents Euclidean distance, and $f_M(\cdot)$ is the nonlinear mapping function for the MPSK signal space normalized on E_s . Applying the bound:

$$Q(\sqrt{x+y}) \leq Q(\sqrt{x}) \exp\left(-\frac{y}{2}\right) \quad x \geq 0, y \geq 0 \quad (5.4)$$

and noticing that

$$d_M^2(X_L, X'_L) - d_{free}^2 \geq 0, \quad (5.5)$$

we can express the pairwise error probability as:

$$\begin{aligned} P(X_L \rightarrow X'_L) &\leq Q\left(d_{free} \sqrt{\frac{E_s}{2N_0}}\right) \exp\left(-\frac{E_s}{4N_0} (d_M^2(X_L, X'_L) - d_{free}^2)\right) \\ &= Q\left(d_{free} \sqrt{\frac{E_s}{2N_0}}\right) \exp\left(\frac{E_s}{4N_0} d_{free}^2\right) \exp\left(-\frac{E_s}{4N_0} \sum_{n=1}^L d_M^2(x_n, x'_n)\right) \\ &= Q\left(d_{free} \sqrt{\frac{E_s}{2N_0}}\right) \exp\left(\frac{E_s}{4N_0} d_{free}^2\right) \prod_{n=1}^L \exp\left(-\frac{E_s}{4N_0} d_M^2(x_n, x'_n)\right). \end{aligned} \quad (5.6)$$

Note that the first two terms in the above expression are independent of X_L and X'_L .

Now, let:

$$T(D) = \sum_{L=1}^{\infty} \sum_{X_L} P(X_L) \sum_{X_L \neq X'_L} \prod_{n=1}^L D^{d_M^2(x_n, x'_n)}, \quad D = \exp\left(-\frac{E_s}{4N_0}\right). \quad (5.7)$$

Referring to (5.1) and (5.6) we can then conclude that:

$$P(e) \leq Q \left(d_{free} \sqrt{\frac{E_s}{2N_0}} \right) D^{d_{free}^2} T(D). \quad (5.8)$$

A close look at (5.7) reveals that it may be possible to find a closed form expression for $T(D)$ using a finite state diagram, as done for the case of linear convolutional codes. In fact, as it will be shown later, for pragmatic trellis codes, $T(D)$ is a scalar *transfer function*.

5.1.1 T(D) and the Error-State Diagram

To find $T(D)$ for TCM schemes, we have to consider all possible paths leaving an arbitrary state p and merging into another state q in exactly L steps for all possible values of L , and error sequences of length L .

Assume that all source symbols have the same probability 2^{-n} . We can then define an $\tilde{N} \times \tilde{N}$ — \tilde{N} is the number of states—*error weight matrix* $G(e_i)$ whose element (p, q) is a function of the distance between the output symbol $x_{p \rightarrow q}$ corresponding to a transition from state p to q , and the same symbol added with noise pattern (e_i) multiplied by the probability of that state transition (or equivalently the source symbol corresponding to that transition). That is :

$$G_{pq}(e_i) = \frac{1}{2^{-n}} \sum_{p \rightarrow q} D^{\|f_M(x_{p \rightarrow q}) - f_M(x_{p \rightarrow q} \oplus e_i)\|^2}. \quad (5.9)$$

In fact, the expression $D^{\|f_M(x_{p \rightarrow q}) - f_M(x_{p \rightarrow q} \oplus e_i)\|^2}$ is an upper bound for the probability of error between the symbols $x_{p \rightarrow q}, (x_{p \rightarrow q} \oplus e_i)$. The series in (5.9) is taken over all possible parallel transitions from state p to state q .

Now, assume that we have an error sequence $E_L = (e_1, e_2, \dots, e_L)$ and calculate the matrix:

$$G(E_L) = \prod_{n=1}^L G(e_n). \quad (5.10)$$

The element (p, q) of this matrix is the probability of a transition from state p to q with an error sequence E_L in exactly L steps. Now if we add all the elements of this matrix, and multiply by the probability of state p ($\frac{1}{N}$ for equiprobable states), we find the probability of error for all possible state transitions corresponding to the error sequence E_L . Finally, if we sum all the probabilities for all possible error sequences of any length, we will have:

$$T(D) = \frac{1}{N} [1]_{1 \times N} \left(\sum_{L=1}^{\infty} \sum_{E_L \neq 0} \prod_{n=1}^L G(e_n) \right) [1]_{N \times 1}, \quad (5.11)$$

where $[1]_{m \times n}$ represents an $m \times n$ matrix all of whose elements are one. The term inside the brackets is called the *matrix transfer function* of the code and is denoted by G .

Moreover, the error vectors in the sequence $E_L = (e_1, e_2, \dots, e_L)$ cannot be treated as independent. In order to take into account their dependence, we can use a state diagram called the *error-state diagram* to describe the connection between the error vectors. It has been proven in [19, p. 107] that the error-state diagram is the exact copy of the state diagram of the code except for its labels. We have to label the error-state diagram with the matrix $G(e_i)$ where e_i is the error pattern for the corresponding transition on the error-state diagram.

Furthermore, in order to find the bit-error probability, the labels of the error-state diagram can be modified to account for the number of erroneous bits in any transition. This can be accomplished by multiplying the elements $G_{pq}(e_i)$ by I^k where k indicates

the number of bits in error for that transition. Note that if there are parallel transitions in the trellis diagram—that is, $G_{pq}(e_i)$ is a series—every element in that series has to be multiplied by the corresponding power of I which are not necessarily equal. Now, if the new function $T(D, I)$ is differentiated with respect to I , and I is set to 1, we will then have the symbol error probability multiplied by n , the number of information bits per channel symbol. Therefore, in order to find the bit-error probability, we must divide the expression by n . In other words:

$$P_b \leq \frac{1}{n} Q \left(d_{free} \sqrt{\frac{E_s}{2N_0}} \right) D^{d_{free}^2} \frac{\partial T(D, I)}{\partial I} \Big|_{I=1}, \quad D = \exp \left(-\frac{E_s}{4N_0} \right). \quad (5.12)$$

As an example, the error-state diagrams of the pragmatic codes of constraint length 3 have the general structure shown in Figure 10. The labels of the error-state diagram are obviously distinct for different rate pragmatic codes, but the general structure is the same—since they differ only in the number of parallel transitions in their trellis diagram. The transfer function of the above error-state diagram is found to be [19]:

$$T(D, I) = \frac{1}{1 - g_4g_5} \left[\frac{g_1g_2g_3g_7}{(1 - g_4g_5)(1 - g_6) - g_2g_3g_5} + g_1g_4g_7 \right]. \quad (5.13)$$

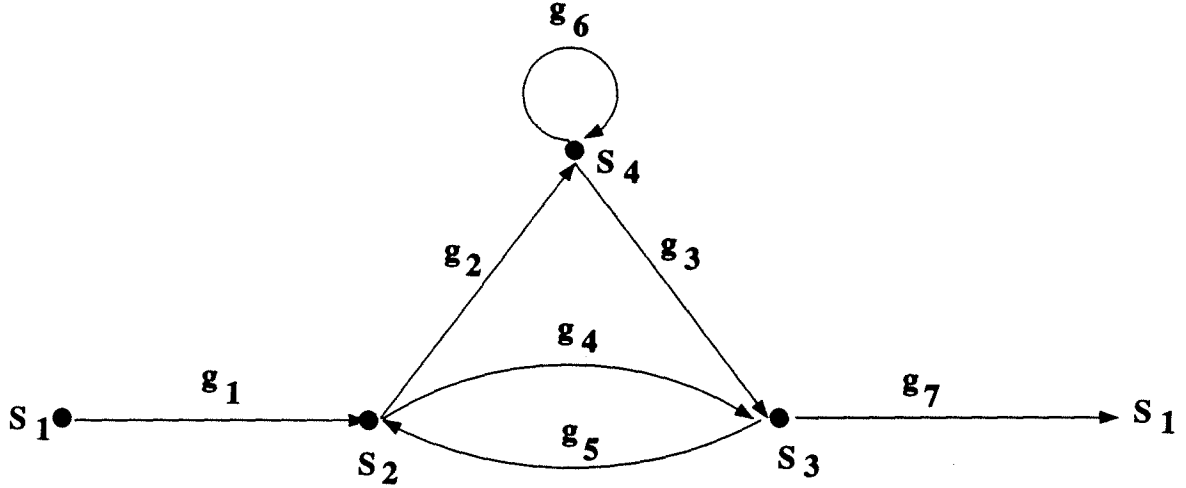


Figure 10 The general structure of the error-state diagram for pragmatic codes ($K=3$).

Note that (5.12) does not take into account the probability of error associated with the single signal error events due to parallel transitions. The transfer function approach will not account for the probability of error due to parallel transition since the transfer function of the error-state diagram takes into account only those transitions going from a certain state to that same state through other states. However, it is possible to find the exact expression for probability of bit-error due to parallel transitions which will be denoted by P_{\parallel} . We will discuss how to find P_{\parallel} later on in this Chapter.

The overall probability of bit-error is the expression found using the transfer function approach plus the probability of error due to parallel transitions. That is:

$$P_b \leq P_{\parallel} + \frac{1}{n} Q \left(d_{free} \sqrt{\frac{E_s}{2N_0}} \right) D^{d_{free}^2} \frac{\partial T(D, I)}{\partial I} \Big|_{I=1}, \quad D = \exp \left(-\frac{E_s}{4N_0} \right), \quad (5.14)$$

where d_{free} is the free distance of the code found ignoring the parallel transitions. d_{free} , together with the minimum distance in parallel transitions, is the most important factor in

the determination of the performance of the code, and can be calculated in many ways . For small constraint lengths, it can be determined by inspections. In fact, if there exists a closed form expression for $T(D, I)$, d_{free} is the smallest exponent of D in the power series expansion of $T(D, I)$. For more complex codes, computational algorithms such as the one explained in [20], [21] can be used. We can also employ a technique which is based on the error-state diagram and its corresponding transfer function. This technique has been explained in sufficient detail in [19, p. 125].

5.1.2 Simplified Error-State Diagram

If all the states are on equal footing, we would expect that the sum of the elements in any row (or column) of the matrix transfer function should be independent of the row (or column) itself. In that case, we can consider only those error events leaving or coming into a certain state without any loss of generality. That is, we can replace matrix labels of the error-state diagram $G(e_i)$ with the sum of the elements in any of its rows (or columns). All calculations can then be carried out in terms of scalars. These scalar labels are called *error-weight profiles* and will be referred to by $W(e_i)$. The algebraic conditions for symmetry are explained in great detail in [22],[19, p. 106]. The set of pragmatic trellis codes satisfy the symmetry condition to the extent that transitions from or to **any state** can be considered without any loss of generality.

5.2 BER Performances of Various Pragmatic TCM Schemes in AWGN

In this section, we derive bounds for BER performance of three pragmatic schemes employed in ATCMPSK; that is:

1. Rate 1/2 TCQPSK

2. Rate 2/3 TC8PSK
3. Rate 3/4 TC16PSK.

All these schemes have the same mother code, and differ in their trellis structure only by the number of parallel branches in their state transitions. The same conventional “good” rate 1/2 encoder is used in all three schemes. For our purposes, and to be consistent throughout this research, we will consider the good rate 1/2 convolutional code of constraint length 3 as the mother code.

The decoder is a slightly modified rate 1/2 Viterbi decoder which first determines the closest symbol to the received symbol among the symbols in every parallel transition, and then operates in the conventional manner.

The method of analysis is that pursued in [19] which can be extended to codes with longer constraint lengths, but theoretical analysis become more complicated with increasing number of states.

5.2.1 Rate 1/2 TCQPSK in AWGN

Figure 11, shows the trellis structure, and the signal space for this scheme. From the trellis diagram we can find the state transition matrix :

$$S = \begin{bmatrix} 00 & 11 & \emptyset & \emptyset \\ \emptyset & \emptyset & 01 & 10 \\ 11 & 00 & \emptyset & \emptyset \\ \emptyset & \emptyset & 10 & 01 \end{bmatrix}. \quad (5.15)$$

The element S_{pq} indicates the output symbol corresponding to a transition from state p to state q . For example, to find S_{11} , see the trellis diagram in Figure 11, and find the output symbol corresponding to the transition from state one (S_1) to itself which in this

case is 00. As another example, the null element (\emptyset) in S_{13} indicates that there is no possible transition from state S_1 to S_3 .

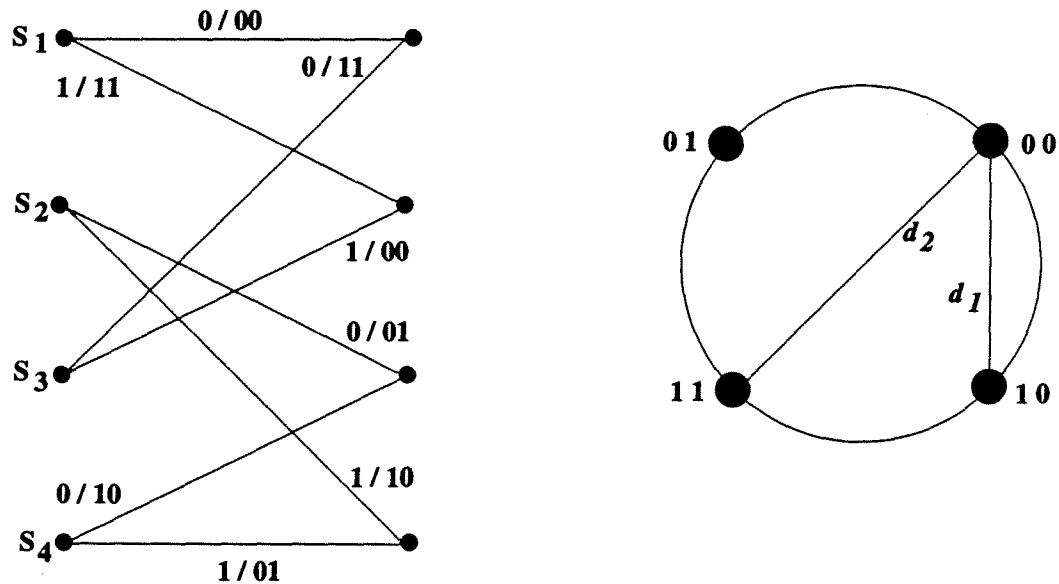


Figure 11 Trellis diagram and the signal space for rate 1/2 TCQPSK.

The next step is to find the error-weight profiles of the code. We can, as discussed before, use the symmetry property and simply consider one state. Assuming that the signal energy is normalized to one, and considering the transitions from state S_1 (the first row of the transition matrix S) the general expression for the error-weight profile $W(e)$ of the rate 1/2 scheme is:

$$W(e) = \frac{1}{2} \left\{ D \|f_4(S_{11}) - f_4(S_{11} \oplus e)\|^2 + D \|f_4(S_{12}) - f_4(S_{12} \oplus e)\|^2 \right\}, \quad (5.16)$$

or equivalently:

$$\begin{aligned}
W(00) &= 1 \\
W(01) &= \frac{1}{2} \left[D \|f_*(00) - f_*(00 \oplus 01)\|^2 + D \|f_*(11) - f_*(11 \oplus 01)\|^2 \right] \\
&= \frac{1}{2} [D^2 + D^2] = D^2 \\
W(10) &= \frac{1}{2} \left[D \|f_*(00) - f_*(00 \oplus 10)\|^2 + D \|f_*(11) - f_*(11 \oplus 10)\|^2 \right] \\
&= \frac{1}{2} [D^2 + D^2] = D^2 \\
W(11) &= \frac{1}{2} \left[D \|f_*(00) - f_*(00 \oplus 11)\|^2 + D \|f_*(11) - f_*(11 \oplus 11)\|^2 \right] \\
&= \frac{1}{2} [D^4 + D^4] = D^4.
\end{aligned} \tag{5.17}$$

Note again that all distances have been normalized to have signal energy equal to one, and the actual energy has been accounted for in the indeterminate D .

Finally, inspecting the trellis diagram, and finding the number of bits in error—power of I —for the transitions on the error-state diagram, we find the labels for the error-state diagram. For example, in order to find g_1 , we find the input symbol for the transition from S_1 to S_2 which is 1 in this case (see Figure 11). Since there is one information bit in error, we multiply the error-weight profile corresponding to that transition, $W(11)$, by I , and that forms the label for the transition in the error-state diagram. Similarly, we find that:

$$\begin{aligned}
g_1 &= W(11)I = D^4 I & g_5 &= W(00)I = I \\
g_2 &= W(10)I = D^2 I & g_6 &= W(01)I = D^2 I \\
g_3 &= W(10) = D^2 & g_7 &= W(11) = D^4 \\
g_4 &= W(01) = D^2.
\end{aligned} \tag{5.18}$$

We can then substitute these labels into (5.13), and perform some algebraic simplifications,

to obtain:

$$T(D, I) = \frac{D^{10}}{(1 - 2D^2I)} = D^{10}I + 2D^{12}I^2 + \dots \quad (5.19)$$

Therefore,

$$\frac{\partial}{\partial I} T(D, I) = \frac{D^{10}}{(1 - 2D^2I)^2} \quad (5.20)$$

Furthermore, from the closed form expression for $T(D, I)$, we find that:

$$d_{free}^2 = 10. \quad (5.21)$$

That is, the smallest exponent of D . Therefore, applying (5.14)—noticing that there are no parallel transitions—we can conclude that:

$$\begin{aligned} P_b &\leq Q \left(\sqrt{\frac{5E_s}{N_0}} \right) \exp \left(\frac{5E_s}{2N_0} \right) \frac{\partial T(D, I)}{\partial I} \Big|_{I=1, D=\exp \left(-\frac{E_s}{4N_0} \right)} \\ &= \frac{Q \left(\sqrt{\frac{5E_s}{N_0}} \right)}{\left(1 - 2 \exp \left(-\frac{E_s}{2N_0} \right) \right)^2} \end{aligned} \quad (5.22)$$

The theoretical upper bound and the simulation results are shown in Figure 12.

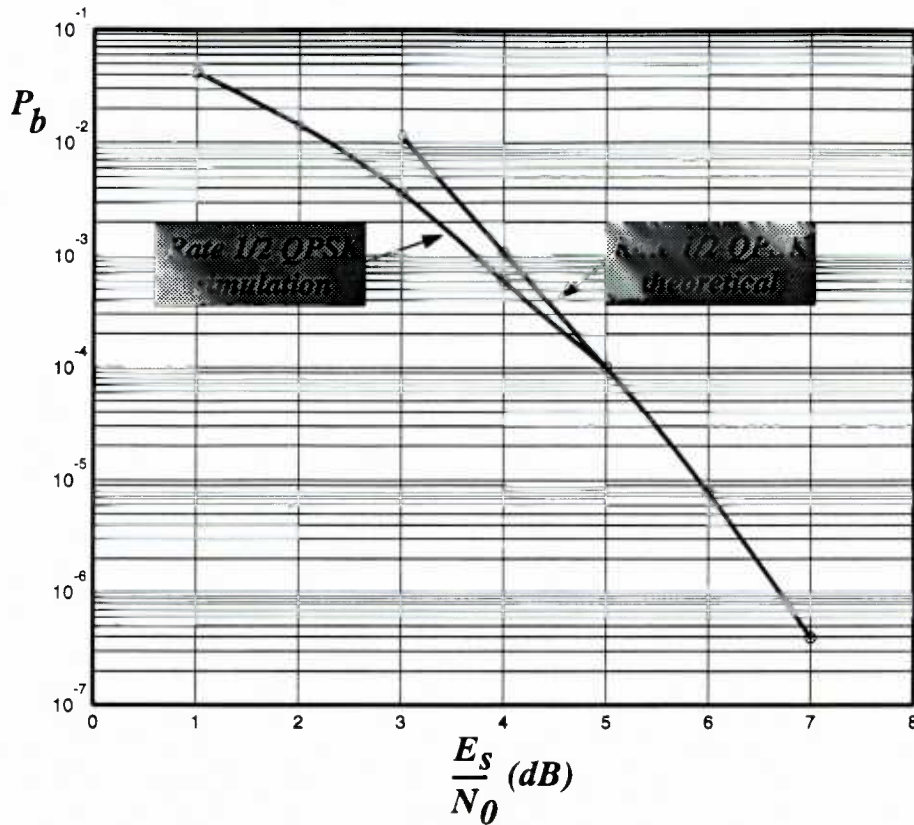


Figure 12 BER Performance of rate 1/2 TCQPSK code in AWGN.

5.2.2 Rate 2/3 TC8PSK in AWGN

In order to find a bound for the BER performance of this scheme, we will follow the same method used for rate 1/2 TCQPSK. The only difference is that now there are parallel branches due to the one extra uncoded bit.

The trellis diagram and the signal space for this scheme are shown in Figure 13.

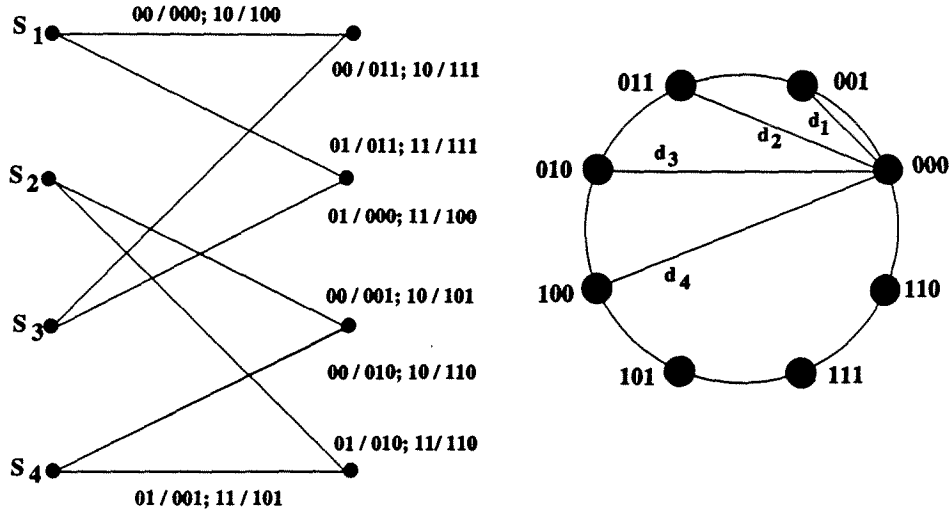


Figure 13 Trellis structure, and the signal space for the rate 2/3 pragmatic code.

From the trellis diagram, we find the state transition matrix:

$$S = \begin{bmatrix} 000; 100 & 011; 111 & \emptyset & \emptyset \\ \emptyset & \emptyset & 001; 101 & 010; 110 \\ 011; 111 & 000; 100 & \emptyset & \emptyset \\ \emptyset & \emptyset & 010; 110 & 001; 101 \end{bmatrix} \quad (5.23)$$

Since there are two parallel transitions in the trellis diagram, every element of the state transition matrix is comprised of two symbols—corresponding to the output symbols of the parallel transitions. The general expression for the error-weight profiles of this scheme is therefore:

$$W(e) = \frac{1}{4} \left\{ \sum_{parallel} D^{\|f_4(S_{11}) - f_4(S_{11} \oplus e)\|^2} + \sum_{parallel} D^{\|f_4(S_{12}) - f_4(S_{12} \oplus e)\|^2} \right\}. \quad (5.24)$$

The error-weight profiles for this scheme, calculated according to (5.24), are given in Table 1.

| Error Pattern (e_i) | Error-Weight Profile $W(e_i)$ |
|-------------------------|---|
| 000 | 1 |
| 001 | $\frac{D^{d_1^2} + D^{d_1^2} + D^{d_1^2} + D^{d_1^2}}{4} = D^{0.586}$ |
| 010 | $\frac{D^{d_3^2} + D^{d_3^2} + D^{d_1^2} + D^{d_1^2}}{4} = \frac{D^{3.414} + D^{0.586}}{2}$ |
| 011 | $\frac{D^{d_2^2} + D^{d_2^2} + D^{d_2^2} + D^{d_2^2}}{4} = D^2$ |
| 100 | $\frac{D^{d_4^2} + D^{d_4^2} + D^{d_4^2} + D^{d_4^2}}{4} = D^4$ |
| 101 | $\frac{D^{d_3^2} + D^{d_3^2} + D^{d_3^2} + D^{d_3^2}}{4} = D^{3.414}$ |
| 110 | $\frac{D^{d_1^2} + D^{d_1^2} + D^{d_1^2} + D^{d_1^2}}{4} = D^{0.586}$ |
| 111 | $\frac{D^{d_2^2} + D^{d_2^2} + D^{d_2^2} + D^{d_2^2}}{4} = D^2$ |

Table 1 Error-weight profiles for the rate 2/3 pragmatic code.

From the trellis diagram, the labels for the error-state diagram are found to be:

$$\begin{aligned}
g_1 &= W(011)I + W(111)I^2 & g_5 &= W(000)I + W(100)I^2 \\
g_2 &= W(010)I + W(110)I^2 & g_6 &= W(001)I + W(101)I^2 \\
g_3 &= W(010) + W(110)I & g_7 &= W(011) + W(111)I \\
g_4 &= W(001) + W(101)I.
\end{aligned} \tag{5.25}$$

Substituting these labels in (5.13) we obtain $T(D, I)$.

By either inspection or the methods described in Section 5.1, we find that :

$$d_{free}^2 = 4.59. \tag{5.26}$$

To find the bit-error probability due to parallel transitions $P_{||}$, note that all states and signals on the branches emanating from those states are on equal footing. Also recall

that the probability of error between two signals separated by a distance d is equal to $Q\left(\frac{d}{\sqrt{2N_0}}\right)$. Now, looking at any branch of the trellis diagram such as the one depicted in Figure 14, we can conclude that:

$$\begin{aligned}
 P_{\parallel} &= \frac{1}{2}P(100 \text{ was received} | 000 \text{ was transmitted}) \\
 &= \frac{1}{2}Q\left(\frac{d(100, 000)}{\sqrt{2N_0}}\right) = \frac{1}{2}Q\left(\frac{2\sqrt{E_s}}{\sqrt{2N_0}}\right) = \frac{1}{2}Q\left(\sqrt{\frac{2E_s}{N_0}}\right).
 \end{aligned} \tag{5.27}$$

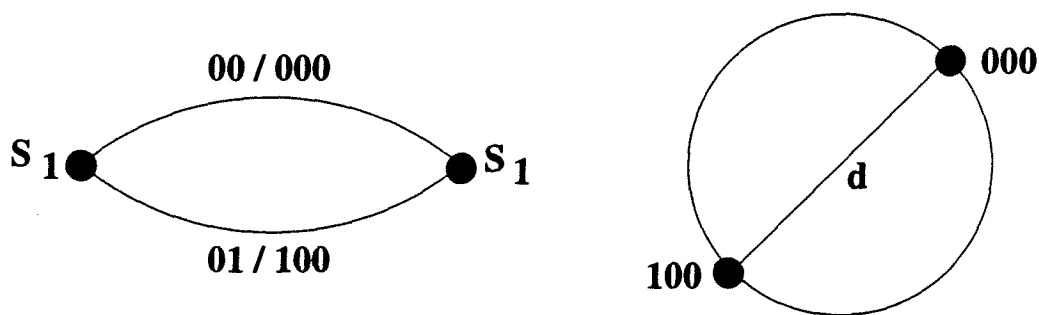


Figure 14 Parallel branches in the trellis for the rate 2/3 code.

Note that the factor 1/2 in the expression for P_{\parallel} stems from the fact that only one bit out of the two information bits would be in error.

Finally, the overall expression for the probability of error can be expressed as:

$$\begin{aligned}
 P_b &\leq \frac{1}{2}Q\left(\sqrt{\frac{4.586E_s}{2N_0}}\right) \exp\left(\frac{4.586E_s}{4N_0}\right) \frac{\partial T(D, I)}{\partial I} \Big|_{I=1; D=\exp\left(-\frac{E_s}{4N_0}\right)} \\
 &\quad + \frac{1}{2}Q\left(\sqrt{\frac{2E_s}{N_0}}\right).
 \end{aligned} \tag{5.28}$$

The expression for the probability of error is complicated, and would not add any insight to the performance of the scheme. Instead, the theoretical curve⁴ for the probability of error, and the corresponding simulation results are shown in Figure 15.

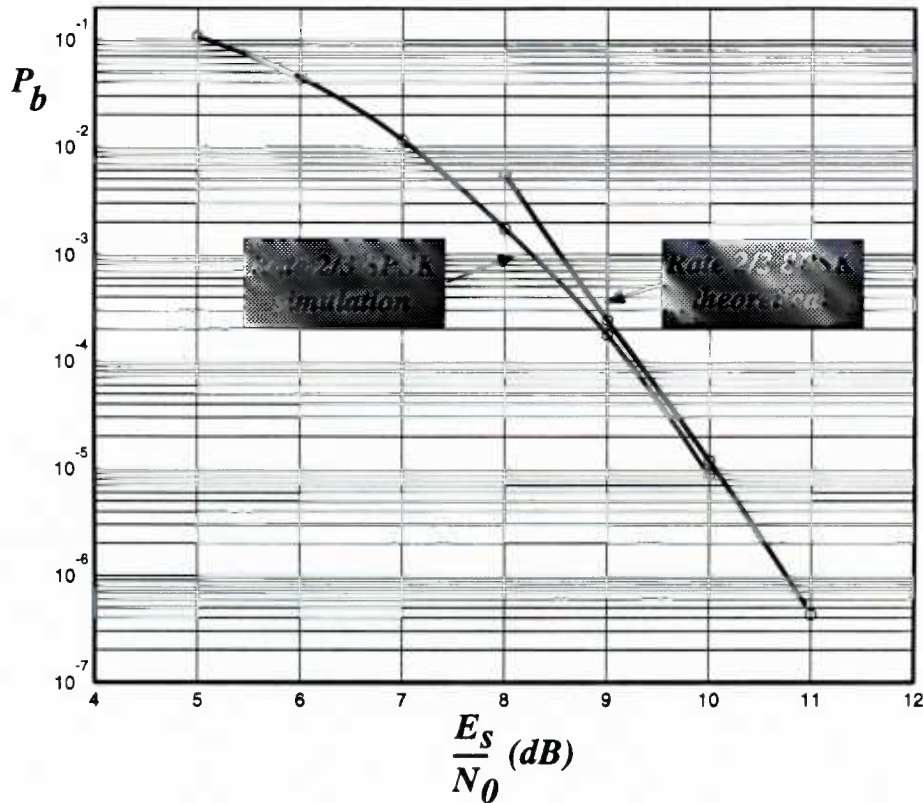


Figure 15 BER performance of the rate 2/3 TC8PSK code in AWGN.

5.2.3 Rate 3/4 TC16PSK in AWGN

The trellis structure and the signal space for this scheme are shown in Figure 16. The same method as for the other two schemes can be applied to find the distance profiles and the labels for the error-state diagram of this scheme.

⁴ The theoretical curves were obtained by carrying out the operations in (5.28) using the symbolic computation program *Maple*.

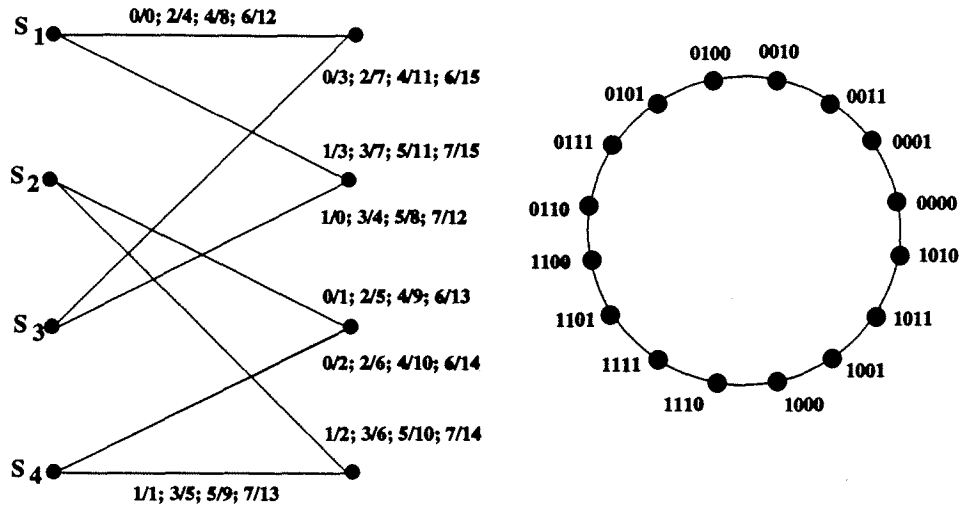


Figure 16 Trellis structure and signal space for rate 3/4 pragmatic code with double-Gray-coded mapping.

Let d_i stand for the distance between two signals separated by i signals. In general, for symmetric MPSK

$$d_i = 2 \sin \left(\frac{i\pi}{M} \right). \quad (5.29)$$

Therefore, for the 16PSK signalling scheme:

$$\begin{aligned} d_1^2 &= 0.152 & d_5^2 &= 2.765 \\ d_2^2 &= 0.586 & d_6^2 &= 3.414 \\ d_3^2 &= 1.235 & d_7^2 &= 3.848 \\ d_4^2 &= 2.000 & d_8^2 &= 4.000 \end{aligned} \quad (5.30)$$

The error weight profiles of the scheme are given in Table 2.

| Error Pattern (e_i) | Error Weight Profile $W(e_i)$ |
|-------------------------|---|
| 0000 | 1 |
| 0001 | $D^{d_1^2}$ |
| 0010 | $\frac{D^{d_1^2} + D^{d_3^2}}{2}$ |
| 0011 | $D^{d_2^2}$ |
| 0100 | $D^{d_4^2}$ |
| 0101 | $\frac{D^{d_3^2} + D^{d_5^2}}{2}$ |
| 0110 | $\frac{D^{d_1^2} + D^{d_3^2} + D^{d_5^2} + D^{d_7^2}}{4}$ |
| 0111 | $\frac{D^{d_2^2} + D^{d_6^2}}{2}$ |
| 1000 | $D^{d_4^2}$ |
| 1001 | $\frac{D^{d_3^2} + D^{d_5^2}}{2}$ |
| 1010 | $\frac{D^{d_1^2} + D^{d_3^2} + D^{d_5^2} + D^{d_7^2}}{4}$ |
| 1011 | $\frac{D^{d_2^2} + D^{d_6^2}}{2}$ |
| 1100 | $D^{d_8^2}$ |
| 1101 | $D^{d_7^2}$ |
| 1110 | $\frac{D^{d_5^2} + D^{d_7^2}}{2}$ |
| 1111 | $D^{d_6^2}$ |

Table 2 Error weight profiles for rate 3/4 pragmatic code with double-Gray-coded mapping.

The labels for the error-state diagram—following the steps explained in the previous section—are found to be:

$$\begin{aligned}
g_1 &= W(0011)I + \{W(0111) + W(1011)\}I^2 + W(1111)I^3 \\
g_2 &= W(0010)I + \{W(0110) + W(1010)\}I^2 + W(1110)I^3 \\
g_3 &= W(0010) + \{W(0110) + W(1010)\}I + W(1110)I^2 \\
g_4 &= W(0001) + \{W(0101) + W(1001)\}I + W(1101)I^2 \\
g_5 &= W(0000)I + \{W(0100) + W(1000)\}I^2 + W(1100)I^3 \\
g_6 &= W(0001)I + \{W(0101) + W(1001)\}I^2 + W(1101)I^3 \\
g_7 &= W(0011) + \{W(0111) + W(1011)\}I + W(1111)I^2
\end{aligned} \tag{5.31}$$

Having determined that:

$$d_{free}^2 = 1.32, \tag{5.32}$$

the bound on BER can be expressed as:

$$P_b \leq P_{||} + Q\left(\sqrt{\frac{1.32E_s}{2N_0}}\right) \exp\left(\frac{1.32E_s}{4N_0}\right) \times \frac{1}{3} \frac{\partial T(D, I)}{\partial I} \Big|_{I=1; D=\exp\left(-\frac{E_s}{4N_0}\right)}. \tag{5.33}$$

To find $P_{||}$, we can once again take advantage of the fact that all transitions are on equal footing and simply look at one transition—the transition from state S_I to itself as shown in Figure 17.

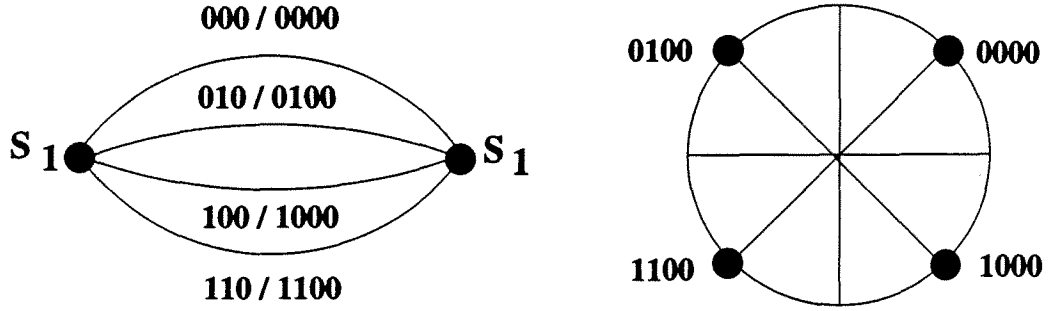


Figure 17 Parallel branches in the trellis diagram of rate 3/4 pragmatic code.

Now, assuming that symbol 0000 was transmitted, we can see that :

$$\begin{aligned}
 P_{\parallel} &= \frac{1}{3}P(0100 \text{ rx'ed}|0000 \text{ tx'ed}) \\
 &+ \frac{1}{3}P(1000 \text{ rx'ed}|0000 \text{ tx'ed}) \\
 &+ \frac{2}{3}P(1100 \text{ rx'ed}|0000 \text{ tx'ed})
 \end{aligned} \tag{5.34}$$

Let $R=(r_1, r_2)$ be the received signal , $X=(x_1, x_2)$ the transmitted signal, and $N=(n_1, n_2)$ the samples of AWGN with zero mean and variance $N_0/2$.

$$\begin{aligned}
 P(0100 \text{ rx'ed}|0000 \text{ tx'ed}) &= P\left(r_1 < 0, r_2 > 0|s_1 = s_2 = \frac{d}{2}\right) \\
 &= P\left(\frac{d}{2} + n_1 < 0, \frac{d}{2} + n_2 > 0\right) = P\left(n_1 < -\frac{d}{2}\right)P\left(n_2 > -\frac{d}{2}\right) \\
 &= Q\left(\frac{\frac{d}{2}}{\sqrt{\frac{N_0}{2}}}\right) \left(1 - Q\left(\frac{\frac{d}{2}}{\sqrt{\frac{N_0}{2}}}\right)\right) = Q\left(\sqrt{\frac{E_s}{N_0}}\right) \left(1 - Q\left(\sqrt{\frac{E_s}{N_0}}\right)\right).
 \end{aligned} \tag{5.35}$$

Equivalently, we have:

$$\begin{aligned}
 P(1000 \text{ rec'ed}|0000 \text{ tx'ed}) &= P(0100 \text{ rec'ed}|0000 \text{ tx'ed}) \\
 &= Q\left(\sqrt{\frac{E_s}{N_0}}\right) \left(1 - Q\left(\sqrt{\frac{E_s}{N_0}}\right)\right),
 \end{aligned} \tag{5.36}$$

and

$$\begin{aligned}
P(1100 \text{ rec'ed} | 0000 \text{ tx'ed}) &= P\left(r_1 < 0, r_2 < 0 | s_1 = s_2 = \frac{d}{2}\right) \\
&= P\left(\frac{d}{2} + n_1 < 0, \frac{d}{2} + n_2 < 0\right) = P\left(n_1 < -\frac{d}{2}\right)P\left(n_2 < -\frac{d}{2}\right) \\
&= Q\left(\frac{\frac{d}{2}}{\sqrt{\frac{N_0}{2}}}\right)^2 = Q\left(\sqrt{\frac{E_s}{N_0}}\right)^2.
\end{aligned} \tag{5.37}$$

Now let $Q\left(\sqrt{\frac{E_s}{N_0}}\right) = p$. We can then express the probability of bit-error due to parallel transitions by:

$$\begin{aligned}
P_{\parallel} &= \frac{1}{3}p(1-p) + \frac{2}{3}p^2 + \frac{1}{3}p(1-p) \\
&= \frac{2}{3}p.
\end{aligned} \tag{5.38}$$

Finally, we can conclude that:

$$P_b \leq \frac{2}{3}p + Q\left(\sqrt{\frac{1.32E_s}{2N_0}}\right) \exp\left(\frac{1.32E_s}{4N_0}\right) \times \frac{1}{3} \frac{\partial T(D, I)}{\partial I} \Big|_{I=1; D=\exp\left(-\frac{E_s}{4N_0}\right)}. \tag{5.39}$$

Figure 18 shows theoretical and simulation results for BER performance of the scheme.

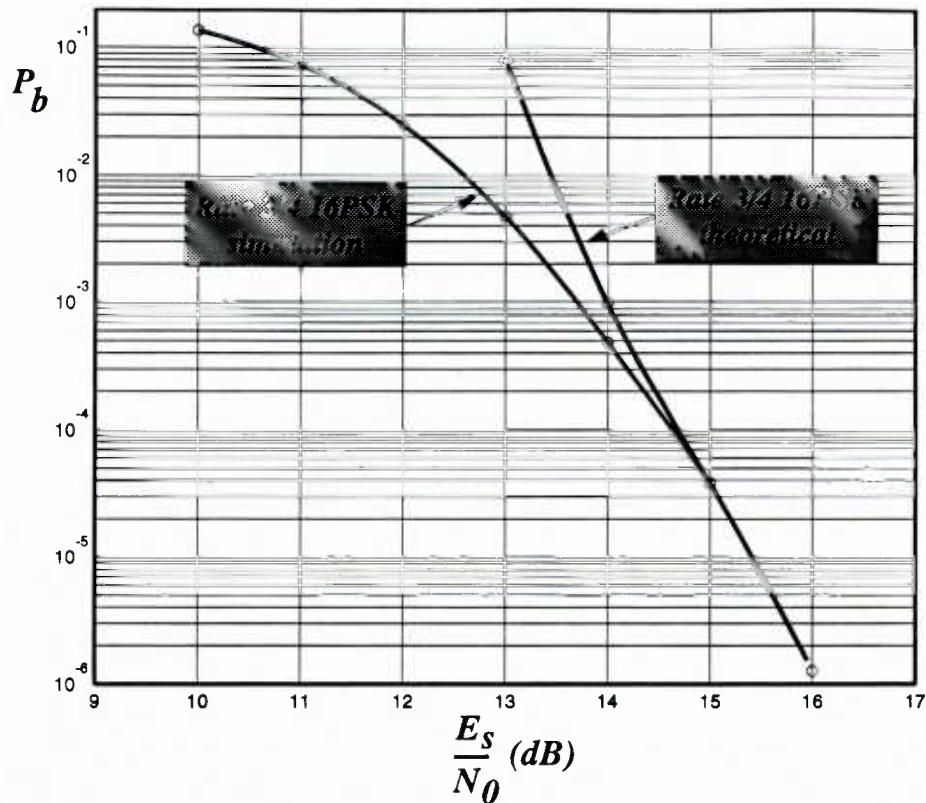


Figure 18 BER performance of rate 3/4 TC16PSK code in AWGN.

5.3 BER Performance of Pragmatic TCM Schemes in the Rayleigh Fading Channel

In order to analyze the error performance of the pragmatic scheme under Rayleigh fading conditions, we will assume the channel model defined in Chapter 3. To keep the analysis as simple as possible the following assumptions are made:

- The channel is frequency nonselective, and slowly fading; therefore, the amplitude of fade is assumed constant for one symbol period or longer.
- The effect of phase is fully compensated for by the receiver.
- Ideal pulse shaping, and hence no ISI.

- Ideal channel state information (CSI) is available at the receiver side. CSI is the amplitude of the fade which is assumed constant over at least one symbol duration.
- Encoded symbols are ideally interleaved, so that the effect of deep fading is spread over time. This assumption allows us to assume that samples of fading are uncorrelated and independent, and that the channel is memoryless.

The first step is to apply the union bound as done for the case of AWGN:

$$P(e|\alpha_1, \alpha_2, \dots, \alpha_\infty) \leq \sum_{L=1}^{\infty} \sum_{X_L} P(X_L) \sum_{X'_L \neq X_L} P(X_L \rightarrow X'_L | \alpha_1, \alpha_2, \dots, \alpha_L). \quad (5.40)$$

Therefore:

$$\begin{aligned} P(e) &\leq E \left[\sum_{L=1}^{\infty} \sum_{X_L} P(X_L) \sum_{X'_L \neq X_L} P(X_L \rightarrow X'_L | \alpha_1, \alpha_2, \dots, \alpha_L) \right] \\ &= \sum_{L=1}^{\infty} \sum_{X_L} P(X_L) \sum_{X'_L \neq X_L} E [P(X_L \rightarrow X'_L | \alpha_1, \alpha_2, \dots, \alpha_L)]. \end{aligned} \quad (5.41)$$

Now, since, as discussed in the last section, the effect of the fading is equivalent to attenuating the signal energy, we have:

$$P(X_L \rightarrow X'_L | \alpha_1, \dots, \alpha_L) = Q \left(\sqrt{\frac{E_s \sum_{n=1}^L \alpha_n^2 d_M^2(x_n, x'_n)}{2N_0}} \right). \quad (5.42)$$

Furthermore, we can use the bound (5.4) to obtain⁵:

$$\begin{aligned}
Q \left(\sqrt{\frac{E_s \sum_{n=1}^L \alpha_n^2 d_M^2(x_n, x'_n)}{2N_0}} \right) &\leq \frac{1}{2} \exp \left(\frac{-E_s \left(\sum_{n=1}^L \alpha_n^2 d_M^2(x_n, x'_n) \right)}{4N_0} \right) \\
&= \frac{1}{2} \prod_{n=1}^L \exp \left(\frac{-E_s (\alpha_n^2 d_M^2(x_n, x'_n))}{4N_0} \right).
\end{aligned} \tag{5.43}$$

Moreover,

$$\begin{aligned}
&E [P(X_L \rightarrow X'_L | \alpha_1, \alpha_2, \dots, \alpha_L)] \\
&= \int_{\alpha_1} \dots \int_{\alpha_L} P(X_L \rightarrow X'_L | \alpha_1, \dots, \alpha_L) f_{\alpha_1, \dots, \alpha_L}(\alpha_1, \dots, \alpha_L) d\alpha_1 \dots d\alpha_L,
\end{aligned} \tag{5.44}$$

and since we have assumed ideal interleaving α_i 's are independent, and identically distributed Rayleigh random variables. That is:

$$f_{\alpha_1, \dots, \alpha_L}(\alpha_1, \dots, \alpha_L) = f_{\alpha_1}(\alpha_1) \dots f_{\alpha_L}(\alpha_L). \tag{5.45}$$

Hence,

$$E [P(X_L \rightarrow X'_L | \alpha_1, \alpha_2, \dots, \alpha_L)] = \prod_{n=1}^L \int_{\alpha_n} \exp \left(\frac{-\alpha_n^2 E_s d_M^2(x_n, x'_n)}{4N_0} \right) f(\alpha_n) d\alpha_n. \tag{5.46}$$

Using the Rayleigh probability density function, we find that:

$$\begin{aligned}
\int_{\alpha} \exp \left(\frac{-\alpha^2 E_s d_M^2(x_n, x'_n)}{4N_0} \right) f(\alpha) d\alpha &= \int_0^{\infty} \exp \left(\frac{-\alpha^2 E_s d_M^2(x_n, x'_n)}{4N_0} \right) 2\alpha e^{-\alpha^2} d\alpha \\
&= \frac{1}{1 + \frac{E_s d_M^2(x_n, x'_n)}{4N_0}}.
\end{aligned} \tag{5.47}$$

⁵ Using the Chernoff bound as done in [19] leads to a bound twice as large.

Substituting the above expression in (5.41) we obtain:

$$P(e) \leq \frac{1}{2} \sum_{L=1}^{\infty} \sum_{X_L} P(X_L) \sum_{X'_L \neq X_L} \prod_{n=1}^L \frac{1}{1 + \frac{E_s}{4N_0} d_M^2(x_n, x'_n)} \quad (5.48)$$

Now, let:

$$T\left(\frac{E_s}{N_0}\right) = \sum_{L=1}^{\infty} \sum_{X_L} P(X_L) \sum_{X'_L \neq X_L} \prod_{n=1}^L \frac{1}{1 + \frac{E_s}{4N_0} d_M^2(x_n, x'_n)} \quad (5.49)$$

$T\left(\frac{E_s}{N_0}\right)$ can be found using the error-state diagram. The labels of the error state diagram must, however, be changed to reflect the effect of fading. In fact, comparing (5.7), the transfer function for the error-state diagram in *AWGN*, with (5.49), we can conclude that in order to obtain $T\left(\frac{E_s}{N_0}\right)$ all one must do is to modify the labels of the error-state diagram—elements of matrices $G(e_i)$ —according to the following transformation:

$$D^{d_M^2(x_n, x'_n)} \rightarrow \frac{1}{1 + \frac{E_s}{4N_0} d_M^2(x_n, x'_n)} \quad (5.50)$$

The corresponding transfer function is no longer an explicit function of D . The labels of the transitions in the error-state diagram in Rayleigh fading are in fact the probability of error for those transitions averaged over the Rayleigh distribution.

Finally, to find the bit-error probability, we have to multiply every transition label by the power of I corresponding to the number of bit errors in that transition. We can then express the overall probability of error by:

$$P_b \leq P_{||} + \frac{1}{2n} \frac{\partial T\left(\frac{E_s}{N_0}, I\right)}{\partial I} \Big|_{I=1} \quad (5.51)$$

The expressions for the probability of error due to parallel transitions P_{\parallel} in AWGN can be used to derive the error probability for the Rayleigh fading channel. In general, if

$$P_{\parallel}\{AWGN\} = g\left(\frac{E_s}{N_0}\right), \quad (5.52)$$

then for the Rayleigh fading channel with ideal CSI we have :

$$P_{\parallel}\{fading|\alpha = \alpha_i\} = g\left(\alpha_i^2 \frac{E_s}{N_0}\right). \quad (5.53)$$

Averaging out the expression over the Rayleigh distribution, we get:

$$\begin{aligned} P_{\parallel} &= E[P_{\parallel}\{fading|\alpha = \alpha_i\}] = E\left[g\left(\alpha_i^2 \frac{E_s}{N_0}\right)\right]. \\ &= \int_0^{\infty} g\left(\alpha^2 \frac{E_s}{N_0}\right) 2\alpha \exp(-\alpha^2) d\alpha. \end{aligned} \quad (5.54)$$

Therefore, using (5.27), we can conclude that for rate 2/3 TC8PSK:

$$\begin{aligned} P_{\parallel} &= \int_0^{\infty} \frac{1}{2} Q\left(\alpha \sqrt{\frac{2E_s}{N_0}}\right) 2\alpha \exp(-\alpha^2) d\alpha. \\ &= \int_0^{\infty} \int_{\alpha \sqrt{\frac{2E_s}{N_0}}}^{\infty} \frac{1}{\sqrt{2\pi}} \exp\left(-y^2 \frac{E_s}{N_0}\right) \alpha \exp(-\alpha^2) dy d\alpha \\ &= \frac{1}{4} \left(1 - \sqrt{\frac{E_s/N_0}{1 + E_s/N_0}}\right), \end{aligned} \quad (5.55)$$

and for rate 3/4 TC16PSK, using (5.38), we find that:

$$\begin{aligned} P_{\parallel} &= 2 \int_0^{\infty} \frac{2}{3} Q\left(\alpha \sqrt{\frac{E_s}{N_0}}\right) \alpha \exp(-\alpha^2) d\alpha. \\ &= \frac{1}{3} \left(1 - \sqrt{\frac{E_s/N_0}{2 + E_s/N_0}}\right) \end{aligned} \quad (5.56)$$

The upper bound for overall probability of error for TC8PSK can therefore be expressed as:

$$P_b \leq \frac{1}{4} \left(1 - \sqrt{\frac{E_s/N_0}{1 + E_s/N_0}} \right) + \frac{1}{2n} \frac{\partial T\left(\frac{E_s}{N_0}, I\right)}{\partial I} \Big|_{I=1} \quad (5.57)$$

and for TC16PSK as:

$$P_b \leq \frac{1}{3} \left(1 - \sqrt{\frac{E_s/N_0}{2 + E_s/N_0}} \right) + \frac{1}{2n} \frac{\partial T\left(\frac{E_s}{N_0}, I\right)}{\partial I} \Big|_{I=1} \quad (5.58)$$

Performance curves for different rate TCMPSK schemes are shown in Figure 19.

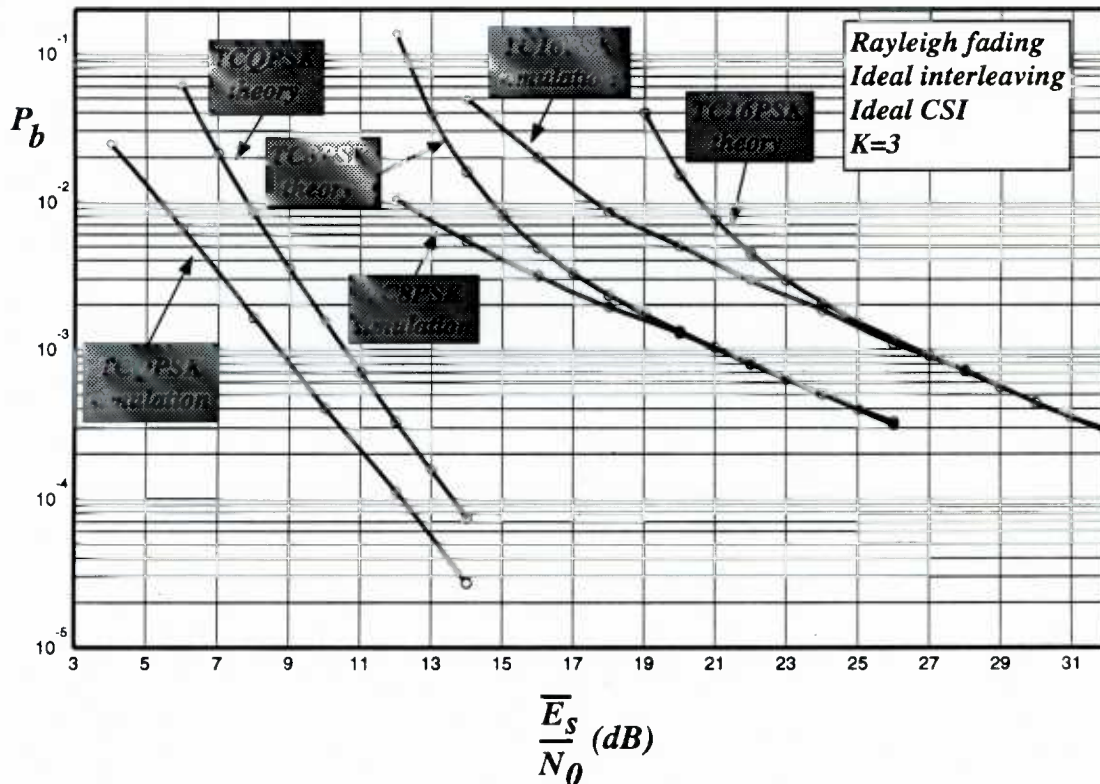


Figure 19 BER performance of ideally interleaved trellis-coded MPSK in Rayleigh fading.

The horizontal axis of Figure 19 is the average SNR which is defined as:

$$\frac{\overline{E_s}}{N_0} = \overline{\alpha^2} \frac{E_s}{N_0} \quad (5.59)$$

As shown in Figure 19, there is a 2 dB asymptotic difference between the simulation⁶ and theoretical BER curves for rate 1/2 TCQPSK. However, for the other two schemes, at high SNR, simulations and theory lead to identical results. This is because the theoretical expressions for $P_{||}$ are exact. Moreover, the overall probability of error is dominated by $P_{||}$. Therefore, at high SNR, the theoretical upper bound on the BER performance of TC8PSK and TC16PSK are almost exact.

⁶ For details regarding the simulations refer to Chapter 7.

Chapter 6

Performance of ATCMPSK in the Rayleigh Fading Channel

6.1 Bound on the BER performance of ATCMPSK in the Rayleigh Fading Channel

For the purpose of theoretical analysis, the assumptions for the nonadaptive case will remain as such. The ATCMPSK scheme under study is the one discussed in Section 4.2. We assume symbol by symbol adaptation. That is, the modulator adjusts its rate according to ideal CSI obtained from the receiver at the start of every symbol transmission interval, and the decoder adjust its parameters at every decoding instant. The metric at every decoding instant is calculated according to the CSI, and is thus a function of the fading amplitude.

The union bound for the probability of error is still valid for the adaptive scheme:

$$P(e) \leq \sum_{L=1}^{\infty} \sum_{X_L} P(X_L) \sum_{X'_L \neq X_L} E[P(X_L \rightarrow X'_L | \alpha_1, \alpha_2, \dots, \alpha_L)]. \quad (6.1)$$

But the conditional probability of an error event of length L is different from the nonadaptive case. The scheme employed at each signalling interval depends on the amplitude of fading in that interval. Let R_n be the number of repetitions for the interval n . The BER performance of a scheme with R_n repetitions and energy E_s is the same as its performance without any repetitions and energy $R_n E_s$. In fact, the effect of repetition is equivalent to increasing the signal energy, and hence a system which adjusts the signal energy according to channel conditions would theoretically have the same BER

performance. Moreover, it is assumed that all R_n symbols are equally attenuated; that is, fading is constant over R_n symbols. This assumption is made only for signalling intervals where repetition schemes are employed. For all other schemes, fading is assumed constant over one symbol period only. Therefore:

$$P(X_L \rightarrow X'_L | \alpha_1, \dots, \alpha_L) = Q \left(\sqrt{\frac{E_s \sum_{n=1}^L R_n \alpha_n^2 d_{M(n)}^2(x_n, x'_n)}{2N_0}} \right), \quad (6.2)$$

Note that $M(n)$ can take on 3 different values: 4 for distances in *QPSK*, and 8, 16 for *8PSK*, and *16PSK*, respectively. Applying the bound (5.4), we obtain:

$$Q \left(\sqrt{\frac{E_s \sum_{n=1}^L R_n \alpha_n^2 d_{M(n)}^2(x_n, x'_n)}{2N_0}} \right) \leq \frac{1}{2} \prod_{n=1}^L \exp \left(\frac{-E_s}{4N_0} R_n \alpha_n^2 d_{M(n)}^2(x_n, x'_n) \right). \quad (6.3)$$

Therefore,

$$E[P(X_L \rightarrow X'_L | \alpha_1, \alpha_2, \dots, \alpha_L)] = \prod_{n=1}^L \int_{\alpha_n} \exp \left(\frac{-E_s}{4N_0} R_n \alpha_n^2 d_{M(n)}^2(x_n, x'_n) \right) f(\alpha_n) d\alpha_n. \quad (6.4)$$

The adaptation thresholds are $\mu_1, \mu_2, \mu_3, \mu_4$. The thresholds have been obtained using the set of BER performance curves of all the different codes in AWGN⁷ so that BER is kept below a certain *error roof* ϵ . To determine the adaptation thresholds in terms

⁷ The way in which these thresholds are chosen is discussed in great detail Section 7.4.1

of the fading amplitude note that:

$$\mu_i \leq \alpha_n^2 \frac{E_s}{N_0} \leq \mu_{i+1} \Rightarrow \sqrt{\frac{\mu_i}{E_s/N_0}} \leq \alpha_n \leq \sqrt{\frac{\mu_{i+1}}{E_s/N_0}}. \quad (6.5)$$

The adaptation thresholds for the fading amplitude are then determined by the relationship $\sqrt{\frac{\mu_i}{E_s/N_0}} = \nu_i$. Therefore, the integral in (6.4) becomes:

$$\begin{aligned} & \int_0^{\nu_1} \exp\left(\frac{-E_s}{4N_0} 3\alpha_n^2 d_4^2(x_n, x'_n)\right) f(\alpha_n) d\alpha_n + \int_{\nu_1}^{\nu_2} \exp\left(\frac{-E_s}{4N_0} 2\alpha_n^2 d_4^2(x_n, x'_n)\right) f(\alpha_n) d\alpha_n \\ & + \int_{\nu_2}^{\nu_3} \exp\left(\frac{-E_s}{4N_0} \alpha_n^2 d_4^2(x_n, x'_n)\right) f(\alpha_n) d\alpha_n + \int_{\nu_3}^{\nu_4} \exp\left(\frac{-E_s}{4N_0} \alpha_n^2 d_8^2(x_n, x'_n)\right) f(\alpha_n) d\alpha_n \\ & + \int_{\nu_4}^{\infty} \exp\left(\frac{-E_s}{4N_0} \alpha_n^2 d_{16}^2(x_n, x'_n)\right) f(\alpha_n) d\alpha_n, \end{aligned} \quad (6.6)$$

where $f(\alpha_n)$ is the Rayleigh density function. Furthermore,

$$\begin{aligned} & \int_{\nu_{i-1}}^{\nu_i} \exp\left(\frac{-R_i \alpha^2 E_s d_n^2(x_n, x'_n)}{4N_0}\right) 2\alpha \exp(-\alpha^2) d\alpha \\ & = \frac{\exp(-\nu_{i-1}^2 \beta_{n,i} E_s/N_0) - \exp(-\nu_i^2 \beta_{n,i} E_s/N_0)}{\beta_{n,i} E_s/N_0} \\ & = \frac{\exp(-\mu_{i-1} \beta_{n,i}) - \exp(-\mu_i \beta_{n,i})}{\beta_{n,i} E_s/N_0}, \end{aligned} \quad (6.7)$$

where

$$\beta_{n,i} = \frac{1}{E_s/N_0} + \frac{R_i d_n^2(x_n, x'_n)}{4}. \quad (6.8)$$

Substituting (6.7) into (6.1) we obtain:

$$\begin{aligned}
P(e) \leq & \frac{1}{2} \sum_{L=1}^{\infty} \sum_{X_L} P(X_L) \sum_{X'_L \neq X_L} \prod_{n=1}^L \\
& \left(\frac{1 - \exp(-\mu_1 \beta_{n,1})}{\beta_{n,1} E_s / N_0} + \frac{\exp(-\mu_1 \beta_{n,2}) - \exp(-\mu_2 \beta_{n,2})}{\beta_{n,2} E_s / N_0} + \right. \\
& \frac{\exp(-\mu_2 \beta_{n,3}) - \exp(-\mu_3 \beta_{n,3})}{\beta_{n,3} E_s / N_0} + \\
& \left. \frac{\exp(-\mu_3 \beta_{n,4}) - \exp(-\mu_4 \beta_{n,4})}{\beta_{n,4} E_s / N_0} + \frac{\exp(-\mu_4 \beta_{n,5})}{\beta_{n,5} E_s / N_0} \right). \tag{6.9}
\end{aligned}$$

Call the term inside the brackets in (6.9) $h(x_n, x'_n)$. We can then express the upper bound on the error-event probability by:

$$P(e) \leq \frac{1}{2} \sum_{L=1}^{\infty} \sum_{X_L} P(X_L) \sum_{X'_L \neq X_L} \prod_{n=1}^L h(x_n, x'_n). \tag{6.10}$$

The right hand side of (6.10) is the generating function $T\left(\frac{E_s}{N_0}\right)$ of the error-state diagram of the adaptive scheme. Comparing it with (5.7), we can conclude that in order to find $T\left(\frac{E_s}{N_0}\right)$, the labels of the error-state diagram for AWGN have to be modified according to the following transformation:

$$D^{d_M^2(x_n, x'_n)} \rightarrow h(x_n, x'_n) . \tag{6.11}$$

Finally, to obtain $T\left(\frac{E_s}{N_0}, I\right)$ we must multiply each term in $h(x_n, x'_n)$ by I^k , where k is the number of bits in error corresponding to that term. The upper bound on BER can then be expressed by:

$$P_b \leq P_{\parallel} + \frac{1}{2\bar{n}} \frac{\partial T\left(\frac{E_s}{N_0}, I\right)}{\partial I} \Big|_{I=1} , \tag{6.12}$$

where \bar{n} is the average number of information bits per adaptation interval, and is equal to:

$$\begin{aligned}
\bar{n} &= P(\text{TCQPSK}) + 2P(\text{TC8PSK}) + 3P(\text{TC16PSK}) \\
&= \int_0^{\nu_3} 2\alpha \exp(-\alpha^2) d\alpha + 2 \int_{\nu_3}^{\nu_4} 2\alpha \exp(-\alpha^2) d\alpha + 3 \int_{\nu_4}^{\infty} 2\alpha \exp(-\alpha^2) d\alpha \\
&= 1 + \exp\left(-\frac{\mu_3}{E_s/N_0}\right) + \exp\left(-\frac{\mu_4}{E_s/N_0}\right).
\end{aligned} \tag{6.13}$$

To find P_{\parallel} we should note that parallel transitions contribute to the probability of error only when channel conditions dictate the use of TC8PSK and TC16PSK. Therefore:

$$P_{\parallel} = \int_{\nu_3}^{\nu_4} \frac{1}{2} Q\left(\alpha \sqrt{\frac{2E_s}{N_0}}\right) 2\alpha e^{-\alpha^2} d\alpha + \int_{\nu_4}^{\infty} \frac{2}{3} Q\left(\alpha \sqrt{\frac{E_s}{N_0}}\right) 2\alpha e^{-\alpha^2} d\alpha. \tag{6.14}$$

Applying (5.4) and integrating the expression above, we find:

$$\begin{aligned}
P_{\parallel} &\leq \frac{1}{4} \frac{e^{-\mu_3 \left(1 + \frac{2}{E_s/N_0}\right)} - e^{-\mu_4 \left(1 + \frac{2}{E_s/N_0}\right)}}{1 + \frac{E_s}{2N_0}} \\
&\quad + \frac{1}{3} \frac{e^{-\mu_4 \left(1 + \frac{1}{E_s/N_0}\right)}}{1 + \frac{E_s}{N_0}}.
\end{aligned} \tag{6.15}$$

Finally, we can express the overall probability of bit-error by:

$$P_b \leq P_{\parallel} + \frac{1}{2\bar{n}} \frac{\partial T\left(\frac{E_s}{N_0}, I\right)}{\partial I} \Big|_{I=1}. \tag{6.16}$$

The BER performance curves obtained by simulations and theory are given in Figure

For the purpose of simulations, a finite interleaving depth of 64×32 was chosen. This interleaving size was found to be almost optimum (see Section 7.4.2.) Furthermore, symbols during repetition periods have been attenuated according to fading at the start of their transmission while for theory we have assumed ideal interleaving of non-repeated symbols and equal attenuation during repetition periods. As expected, the upper bound is fairly accurate at high SNR where it is 2 dB away from the simulation results.

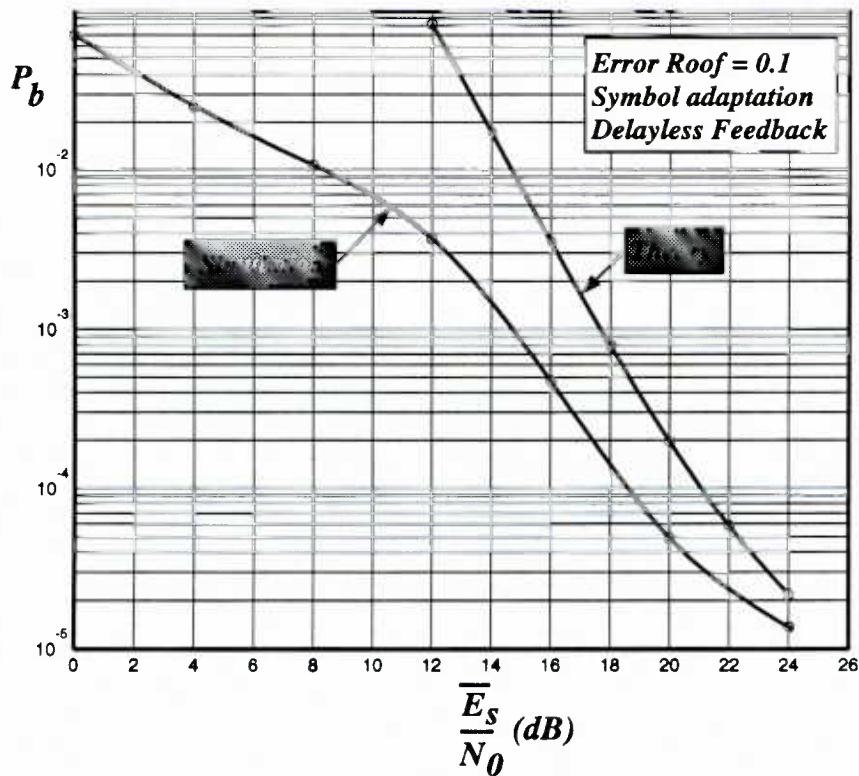


Figure 20 Theoretical and simulation curves for the BER performance of ATCMPSK under Rayleigh Fading.

6.2 Throughput of ATCMPSK

Due to its adaptive nature, the throughput of the ATCMPSK scheme will vary as a function of the immediate SNR. The throughput can be defined as the average number of information bits transmitted per symbol duration T_s .

But the number of information bits per channel symbol is 1/3 for QPSK with three repetitions, 1/2 for QPSK with two repetitions, one for TCQPSK, two for TC8PSK, and three for TC16PSK. Therefore:

$$\begin{aligned} \bar{\eta} = & \frac{1}{3}P(0 \leq \alpha \leq \nu_1) + \frac{1}{2}P(\nu_1 \leq \alpha \leq \nu_2) + P(\nu_2 \leq \alpha \leq \nu_3) \\ & + 2P(\nu_3 \leq \alpha \leq \nu_4) + 3P(\nu_4 \leq \alpha \leq \infty). \end{aligned} \quad (6.17)$$

Assuming that there is no correlation between adjacent transmission periods with regards to the choice of throughput, and using the fact that samples of fading are Rayleigh distributed, we have that:

$$P(\nu_i \leq \alpha \leq \nu_{i+1}) = \exp(-\nu_i^2) - \exp(-\nu_{i+1}^2). \quad (6.18)$$

Recall that

$$\nu_i = \sqrt{\frac{\mu_i}{E_s/N_0}}, \quad (6.19)$$

where μ_i 's are the adaptation thresholds found from the performance of the different schemes in AWGN. The throughput of the proposed ATCMPSK can hence be expressed as:

$$\begin{aligned} \bar{\eta} = & \frac{1}{3} + \frac{1}{6} \exp\left(-\frac{\mu_1}{E_s/N_0}\right) + \frac{1}{2} \exp\left(-\frac{\mu_2}{E_s/N_0}\right) \\ & + \exp\left(-\frac{\mu_3}{E_s/N_0}\right) + \exp\left(-\frac{\mu_4}{E_s/N_0}\right). \end{aligned} \quad (6.20)$$

The above expression has been derived by treating every symbol transmission period as independent from its adjacent neighbours. This is true when there are no repetitions used. However, when repetition schemes are employed the adjacent repeated symbols

are not independent; however, since we have slow fading, this does not effect the overall expression for throughput, and the approximation is hence very accurate.

Note that, for very small SNR, the above expression approaches 1/3 (the throughput of the triple repetition TCQPSK scheme), and for very high SNR it approaches 3 (the throughput of the TC16PSK scheme).

In general, for a system employing up to R repetitions and 2^{n+1} PSK, the throughput can be expressed as:

$$\bar{\eta} = \frac{1}{R} + \sum_{i=0}^{R-2} \frac{\exp\left(-\frac{\mu_{i+1}}{E_s/N_0}\right)}{(R-i)(R-i-1)} + \sum_{i=0}^{n-2} \exp\left(-\frac{\mu_{R+i}}{E_s/N_0}\right). \quad (6.21)$$

Throughput curves obtained by simulations and theory are given in Figure 21. The curves overlap since theoretical results are almost exact—there is a negligible discrepancy which is attributed to the correlation between the adjacent symbols during repetition periods which has been ignored in theory.

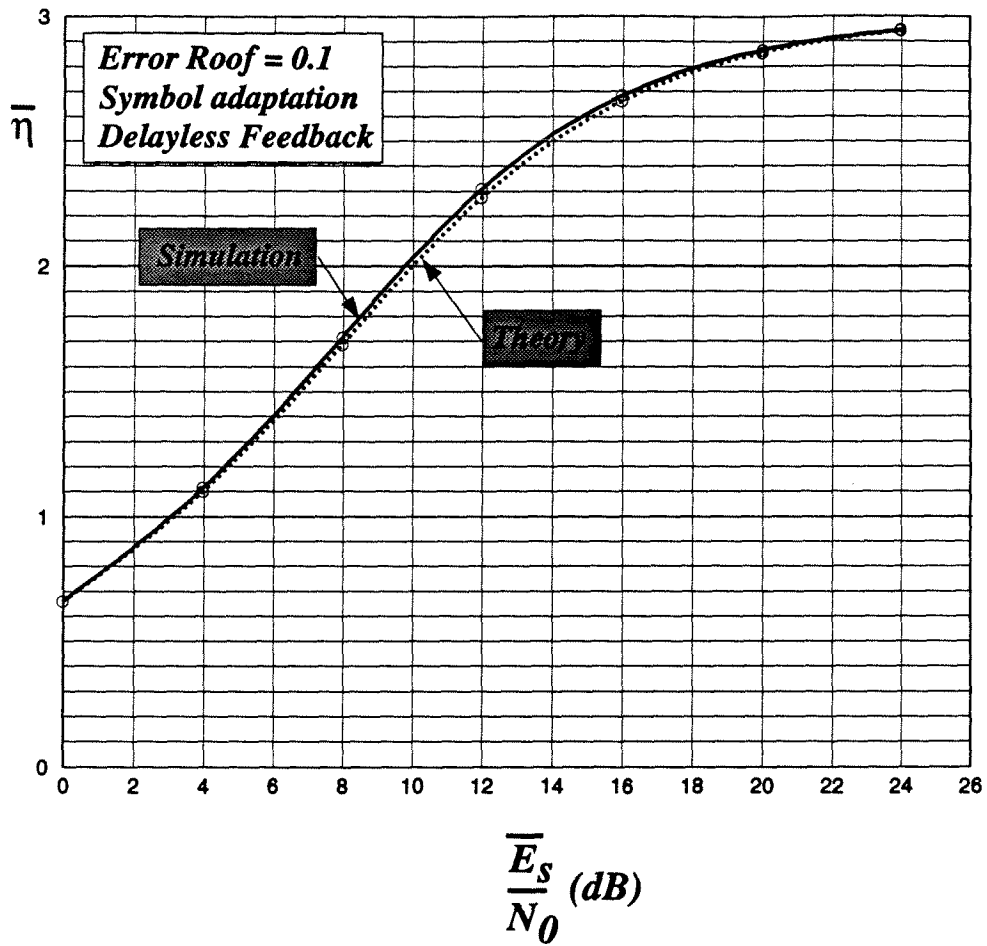


Figure 21 Information throughput of ATCMPSK—simulation and theory.

Chapter 7

Description of Computer Simulations

7.1 The AWGN Channel

All simulations have been carried out in baseband, and the overall transfer function of the transmit and received filters was assumed to satisfy Nyquist's first criterion for pulse transmission; that is, there is no ISI at the sampling instant. Therefore, the effect of the AWGN on the transmitted signal can be modelled in the following manner.

Assume that (s_{i1}, s_{i2}) is the baseband equivalent of the transmitted signal. The baseband representation of the received signal is hence:

$$(r_{i1}, r_{i2}) = (s_{i1} + n_{i1}, s_{i2} + n_{i2}) \quad (7.1)$$

where n_{i1}, n_{i2} are two independent Gaussian random variables with zero mean and variance $N_0/2$.

In our simulations, to generate a sequence of AWGN samples, the Gaussian random generator routine in [23, p. 217] together with the whitening procedure in [23, p. 207] were used. The first routine generates an array of independent Gaussian noise samples. In all the simulations performed for the purpose of this thesis, the length of this array was chosen as 10000. Whenever the simulations run out of noise samples, a whole new array is generated. The seed used for the random number generator is the μsec field of the time function in the *C* library.

The simulated signal space has unit energy ($E_s=1$). The variance of Gaussian noise to operate at a certain SNR is hence determined as follows:

$$\sigma^2 = \frac{N_0}{2}, \quad SNR = \frac{E_s}{N_0} = \frac{1}{N_0}. \quad (7.2)$$

Therefore

$$\sigma^2 = \frac{1}{2SNR}. \quad (7.3)$$

7.2 The Rayleigh Fading Channel

The following assumptions were made in the simulation of the Rayleigh fading channel:

1. The effect of fading on the phase of the transmitted signal is not included in the model. It has been assumed, as in the derivation of the theoretical bounds, that the effect of phase has been fully compensated for.
2. Unless indicated otherwise, the carrier frequency f_c has been chosen as 864 MHz, and the Baud rate as 10000 symbols/sec or equivalently the symbol duration $T_s = 0.1$ msec. Therefore,

$$\begin{aligned} B_d &= \frac{v}{c} f_c = 0.8v, \\ B_d T_s &= 8 \times 10^{-5} v \end{aligned} \quad (7.4)$$

where B_d is the *maximum Doppler shift*, v is the speed of the vehicle, and c is *propagation speed* assumed equal to the speed of light— $10^8 \times 10^7$ km/hr.

3. It is assumed that fading is sufficiently slow so that it can be considered constant at least during one symbol interval. That is, the symbol duration T_s is much smaller

than the coherence time of the channel defined as $(\Delta t)_c = \frac{1}{B_d}$, or equivalently:

$$\begin{aligned} 8 \times 10^{-5} v &<< 1 \text{ or} \\ v &<< 10^4 \text{ km/hr.} \end{aligned} \quad (7.5)$$

4. The attenuation during one symbol period is the value of fading at the start of each transmission.
5. Unlike the theory, the signals transmitted during a repetition period are faded according to channel conditions at the start of each symbol transmission.

According to these assumptions, the received signal can be modelled by:

$$(r_{i1}, r_{i2}) = (\alpha_i s_{i1} + n_{i1}, \alpha_i s_{i2} + n_{i2}), \quad (7.6)$$

where the samples of fading α_i 's are generated according to Jakes' model of Rayleigh fading channel.

7.2.1 Jakes' Model of Rayleigh Fading (Land-Mobile)

Jakes [8] showed that the in-phase and quadrature components of the envelope of the fading signal can be expressed by:

$$\begin{aligned} x_c(t) &= 2 \sum_{n=1}^{\hat{N}_0} \cos\left(\frac{\pi n}{\hat{N}_0}\right) \cos(2\pi f_n t) + \cos(2\pi f_m t), \\ x_s(t) &= 2 \sum_{n=1}^{\hat{N}_0} \sin\left(\frac{\pi n}{\hat{N}_0}\right) \cos(2\pi f_n t) + \cos(2\pi f_m t). \end{aligned} \quad (7.7)$$

f_m is the maximum Doppler frequency, and

$$\begin{aligned} f_n &= f_m \cos \frac{2\pi n}{\hat{N}}, \quad n = 1, 2, \dots, \hat{N}_0 \\ \hat{N} &= 4\hat{N}_0 + 2. \end{aligned} \quad (7.8)$$

N_0 ⁸ is the number of low frequency oscillators needed to effectively simulate the multipath effect. It has been shown in [8, p. 69] that 8 oscillators are sufficient for this purpose.

A sample of fading at time kT_s can be expressed by:

$$\alpha(kT) = \sqrt{x_c^2(kT) + x_s^2(kT)}. \quad (7.9)$$

We have [8, p. 72]:

$$\begin{aligned} E[x_c^2(t)] &= \hat{N}_0 + 1, \\ E[x_s^2(t)] &= \hat{N}_0, \end{aligned} \quad (7.10)$$

or equivalently:

$$E[x_c^2(t) + x_s^2(t)] = 2\hat{N}_0 + 1. \quad (7.11)$$

Therefore, in order to normalize the fading energy to one, we must have:

$$\alpha(kT) = \sqrt{\frac{x_c^2(kT) + x_s^2(kT)}{2\hat{N}_0 + 1}}. \quad (7.12)$$

The block diagram of the baseband fading simulator is shown in Figure 22. The model was simulated using the *C* programming language.

In order to simulate ideal interleaving, one can simply choose $x_c(t)$, $x_s(t)$ to be two independent Gaussian random numbers with zero mean and variance 0.5, hence removing the correlation between the symbols transmitted over the channel. The Gaussian random generator explained in the last section was used to generate all the Gaussian numbers needed for this purpose.

⁸ Note that in this section N_0 does not represent the AWGN spectral density.

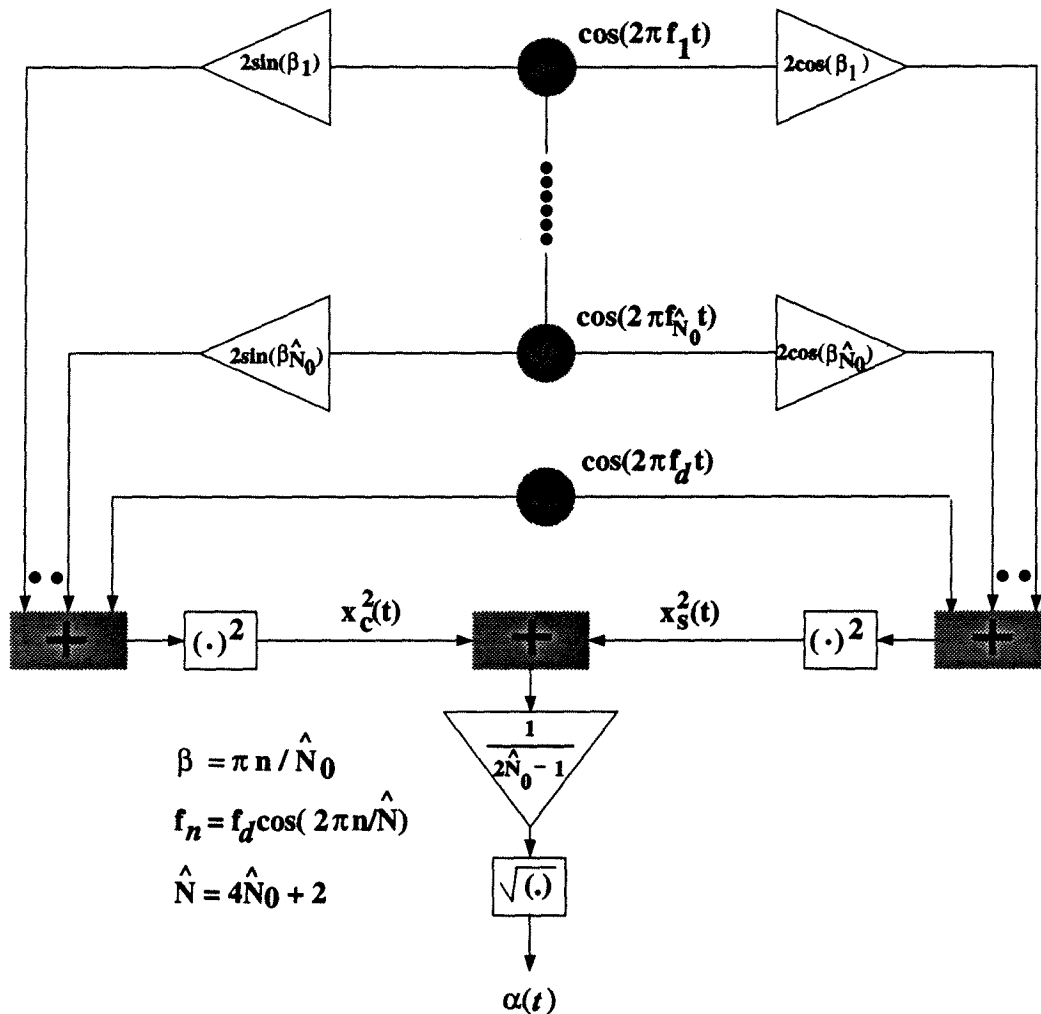


Figure 22 Block diagram of the baseband land-mobile fading simulator.

7.3 Simulation of the codulator/decodulator

We have chosen an encoder of constraint length three, and a decoding depth of 18 (six times the constraint length of code [18].) It was verified, by means of computer simulations, that for all practical purposes the coding loss due to the finite decoding depth is negligible for a decoding depth of 18.

Information bits are generated using the *C* library function *lrand48* which returns a positive long integer in the interval $[0, 2^{31}]$. The 18th least significant bit of the returned integer value is chosen as the random bit. The modulation scheme to be used is determined according to the value of the immediate SNR. It is assumed that CSI is available to both the encoder and the decoder. The encoder is a rate 1/2 convolutional encoder with extra inputs for uncoded bits. Changing the coding rate is equivalent to varying the number of uncoded bits per symbol. Encoded symbols are then mapped into the MPSK signal space with unit energy. If channel conditions indicate the use of repetitions, the transmitter repeats the modulated symbol R times. Note that in the theoretical analysis we assumed that repeated symbols are faded equally. For the purpose of simulations, however, a more realistic model is used, and the repeated signals are attenuated at each signalling period by the fading component in that period.

The decoder has ideal CSI, and is aware of the modulation scheme employed for any received signal since the request has been made at the receiver side. The decoder makes its first decision on parallel branches of the trellis by choosing the closest signal to the received signal. The metric used is Gaussian metric which, for any state, and at each decoding instant is normalized with respect to the smallest metric for that state. The values of the state metrics are not quantized. The decoder has to store past information about state transitions, and input symbols leading to those transmissions in a history array whose size is determined by the decoding depth. Finally, decoded symbols and corresponding information symbols are compared, and the BER performance of the scheme is determined.

7.4 Performance Evaluation Results

7.4.1 Effect of Error Thresholds on the BER Performance and Throughput

As it was discussed before, the adaptation thresholds were chosen in a way as to keep the BER below an error roof. Performance curves of the scheme in AWGN were used to determine the thresholds for changing from one scheme to another. Figure 23 depicts this concept.

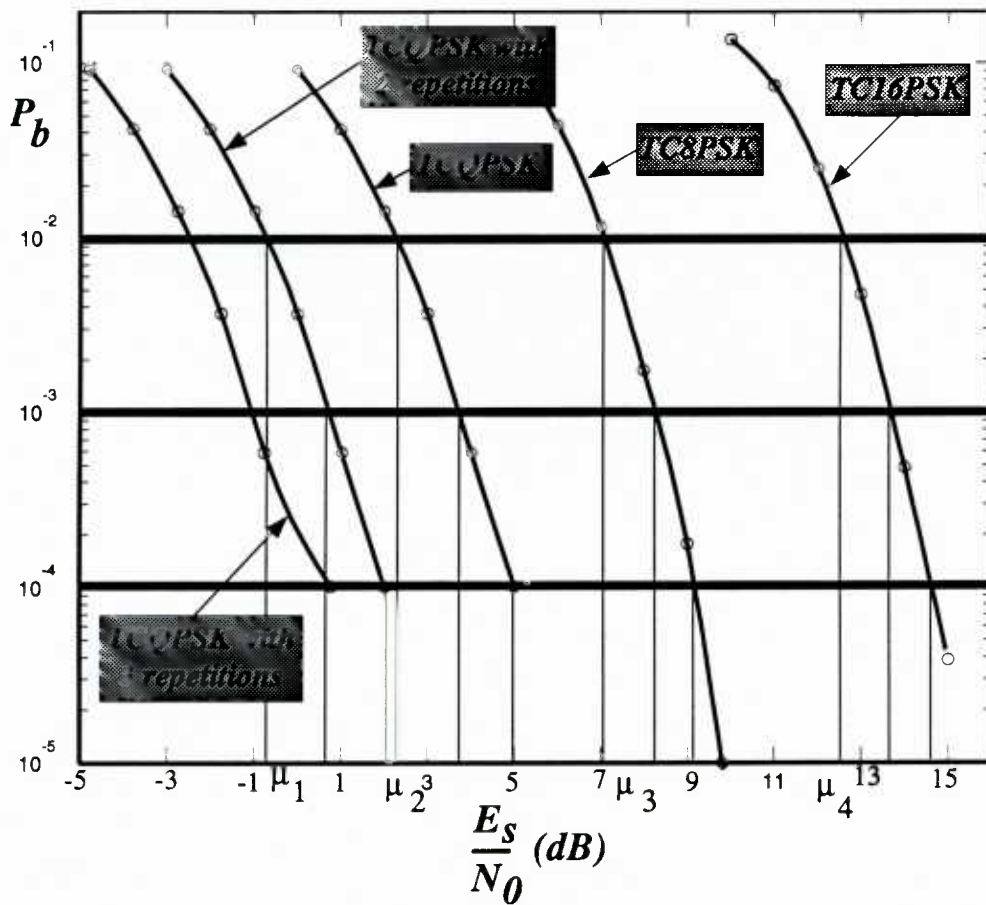


Figure 23 Adaptation thresholds for ATCMPSK.

As the error roof is lowered further, the thresholds for all scheme move towards the right. That is, schemes with worse BER performance and higher throughput are employed at higher SNR. This will result in a better overall BER performance but lower throughput. For high SNR, however, the difference in throughput between two schemes with different error roofs becomes very small while the BER performance remains significantly different.

Moreover, as the error roof is lowered, slopes of the performance curves approach infinity, and, therefore, further lowering of the roof will not have any effect on the thresholds. Figure 24 shows the BER performance of ATCMPSK with different error roofs.

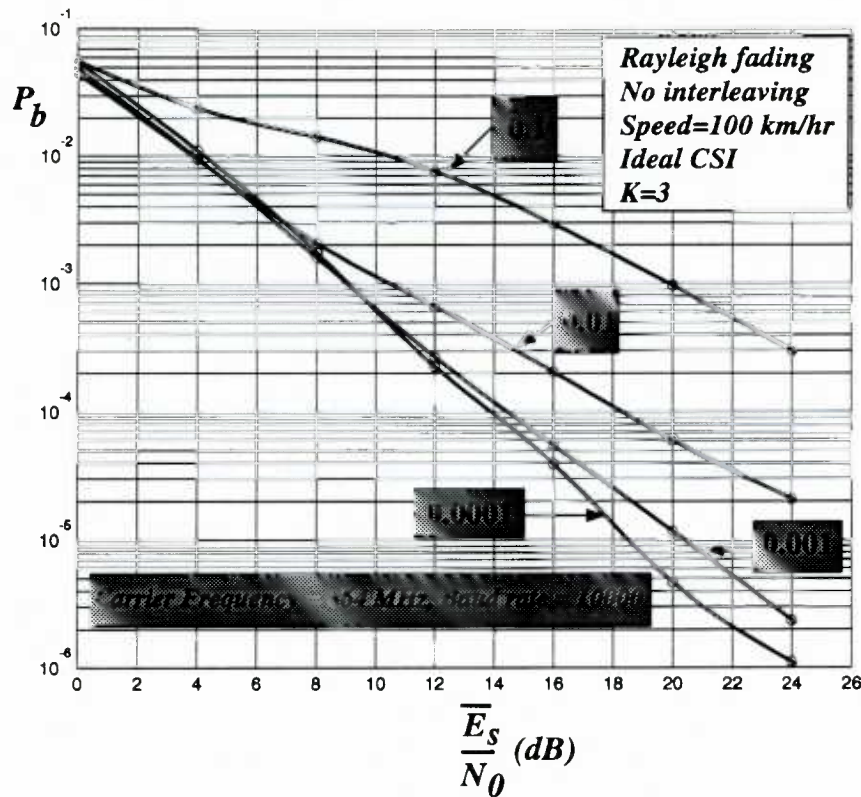


Figure 24 BER performance of ATCMPSK with different error roofs.

It can be seen that BER performance of the scheme using an error roof of 0.1 and those using lower roofs are significantly different. However, as the roof is lowered, the difference becomes smaller and smaller—up to the point where the thresholds overlap and the performance remains constant.

The throughput curves for schemes using different error roofs are shown in Figure 25.

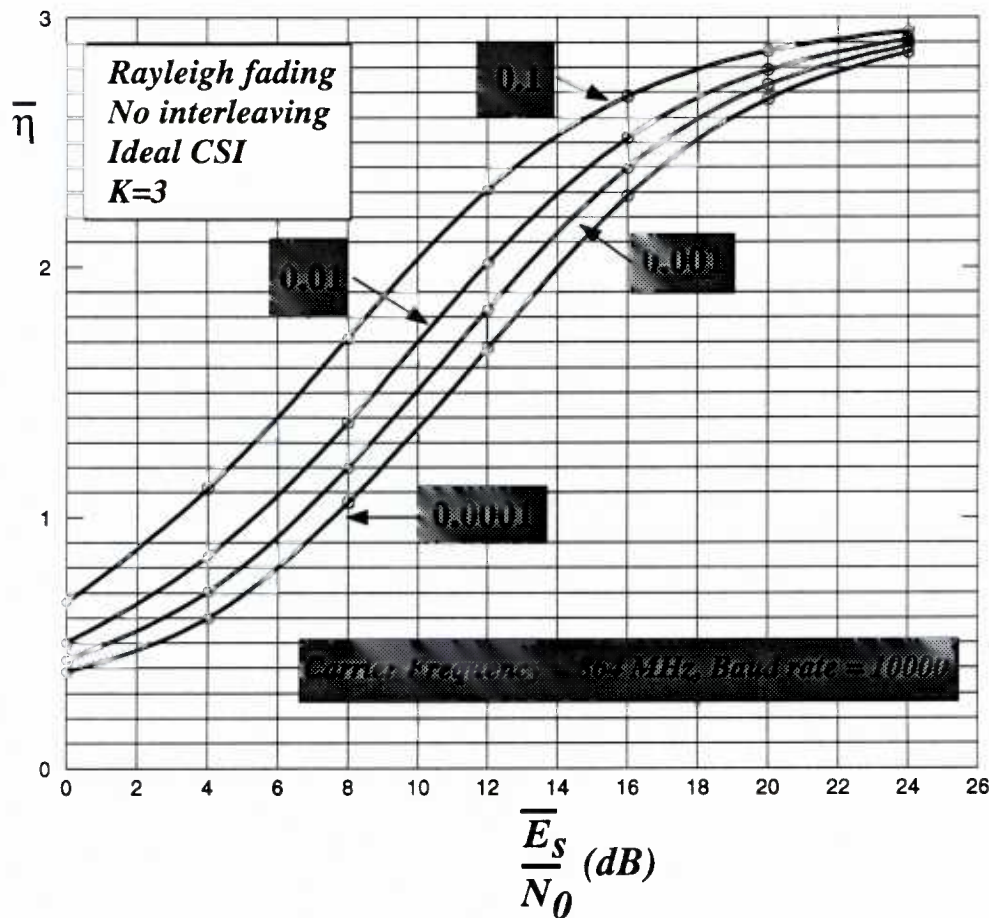


Figure 25 Throughput of ATCMPSK for different error roofs.

As expected, the throughput of the schemes using larger error roofs is significantly better than those with smaller ones. Therefore, the question: “what are the optimum thresholds?” is not easy to answer. In fact, because of the trade-off between error

performance and throughput, it is impossible to quantify the difference between two schemes using different error roofs. One can observe the BER and throughput curves at a certain SNR and decide which one is more suitable for a certain application. However, at high SNR the difference between throughputs becomes small while the difference between BER performances is still significant. Therefore, if the system is to operate at high SNR, it is better to use a relatively small error roof.

Introducing error roofs is not the only possible way of choosing the thresholds. In fact, we can obtain an infinite family of performance and throughput curves within the constraints that bound the error performance and the throughput. We can shape the performance curves in any way we wish—within those constraints.

7.4.2 Effect of Finite Interleaving

As discussed before, the effect of interleaving is the same as removing the correlation between adjacent symbols on the trellis diagram. As the interleaving depth is increased, the correlation between adjacent symbols is reduced until any further increase would not result in any more improvement. BER performance of ATCMPSK with an error roof of 0.01 and different interleaving depths are given in Figure 26. It is evident that interleaving results in considerable improvement in performance. The interleaving depth of 32 proved to be nearly optimum for the specific example shown above. It was verified that an interleaving depth of 64 does not result in any further improvement.

It is important to note that the improvement resulting from interleaving is more significant at high values of SNR. This is because, at low SNR, the distortion due to the AWGN is more prevalent while at high SNR it becomes almost negligible. At high

SNR, therefore, the major reason for distortion is the attenuation due to fading whose contribution to BER can be reduced by interleaving.

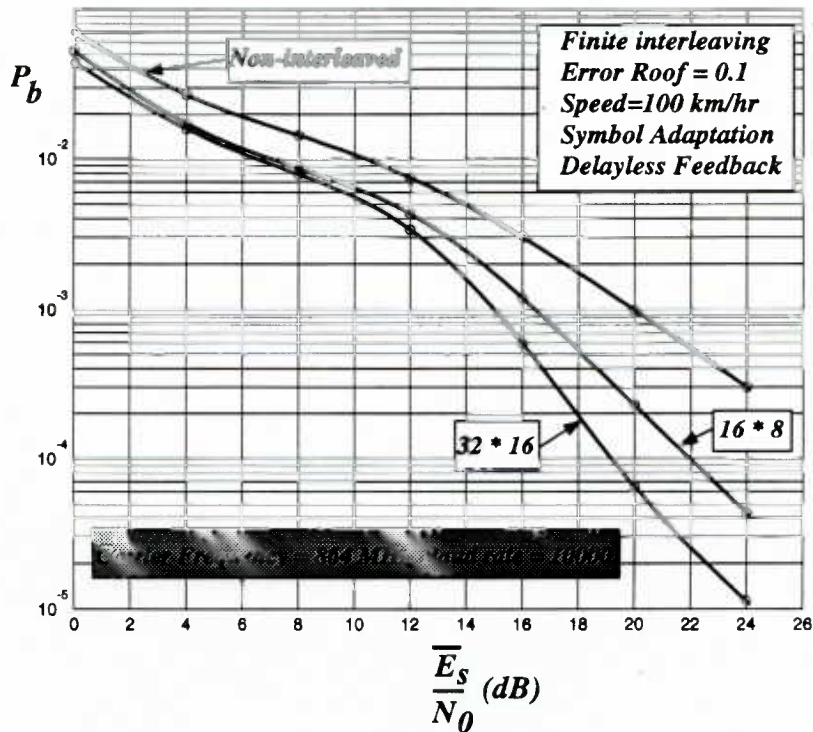


Figure 26 Effect of finite interleaving on BER performance of ATCMPSK.

7.4.3 Comparison of ATCMPSK with Nonadaptive TCM Schemes

BER performance curves for ATCMPSK with an error roof of 0.01, and the fixed rate 1/2 TCQPSK are given in Figure 27. Included in the same graph is the throughput curve for the adaptive schemes⁹.

⁹ Confidence intervals for the least accurate points of the BER performance curves for ATCMPSK are given in Appendix C.

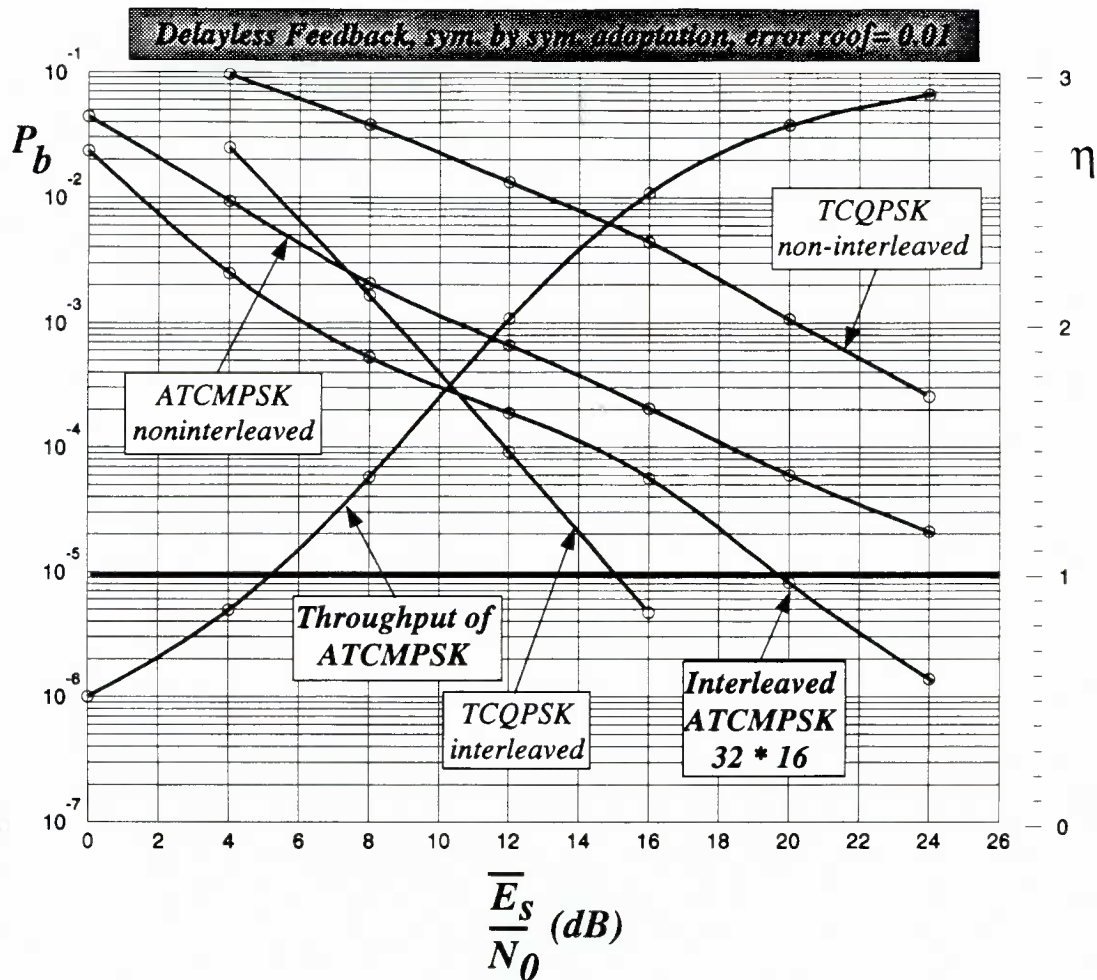


Figure 27 BER curves for ATCMPSK and fixed rate TCQPSK, with superimposed curve of the throughput performance of ATCMPSK.

As shown in Figure 27, there is a lot to be gained through interleaving in either ATCMPSK or TCQPSK. It is also evident that interleaved ATCMPSK is significantly better in terms of BER performance. To quantify the gain, we can look at the point where the BER curves of interleaved ATCMPSK and TCQPSK meet. This occurs at 10.5 dB, where the throughput of ATCMPSK is almost 1.8. That is, for the same BER the information throughput has almost doubled. We can look at the gain in a different way. The throughput of the ATCMPSK increases monotonically with SNR, and

at $SNR \approx 5.2 \text{ dB}$ it becomes equal to one which is the throughput of TCQPSK. At that SNR, the BER of the adaptive scheme is around 10^{-3} while TCQPSK has a BER of 10^{-2} . That is, we have a BER improvement of almost one order of magnitude for the same throughput. Yet another way of comparing the performances is to find the SNR at which the performance of TCQPSK is the same as that of ATCMPSK with a throughput of one. We find that this happens at about 8.5 dB. Hence, we can conclude that there is more than 3 dB gain for the special case of interleaved ATCMPSK with an error roof of 0.01.

Now, if we compare the noninterleaved versions of both schemes, we see that the BER curves are almost parallel, with the adaptive scheme 8 – 10 dB better than the fixed rate code. At the first glance, this may seem unusual and contrary to common sense. One could—wrongly—suggest that since at high SNR most of the channel uses in the adaptive scheme are TC16PSK, then a better scheme such as TCQPSK should eventually become better in terms of its BER performance. However, this suggestion is not true. The reason for this is a phenomenon that can be called *error leakage*. It is obvious that occurrence of errors at high SNR are due to deep fades. It is also true that at high SNR the prevailing scheme with regards to the number of channel usage is the highest rate code TC16PSK. However, most errors for fixed rate TCQPSK happen at very low immediate SNR values at which ATCMPSK uses the least prevalent schemes; that is, TCQPSK with repetitions, which are superior to single transmission of TCQPSK signals. To clarify this point, the details of the error events that have contributed to the BER of the noninterleaved ATCMPSK—shown in Figure 27—are given in Table 3.

| Scheme | Number of Channel uses | Number of bits in error | Percentage of Total usage | Percentage of total errors |
|------------------------------|------------------------|-------------------------|---------------------------|----------------------------|
| <i>TCQPSK 3 repetitions</i> | 23569 | 65 | 0.12% | 6.7% |
| <i>TCQPSK 2 repetitions</i> | 37374 | 21 | 0.19% | 2.2% |
| <i>TCQPSK no repetitions</i> | 227752 | 49 | 1.1% | 5.3% |
| <i>TC8PSK</i> | 919350 | 244 | 4.6% | 25% |
| <i>TC16PSK</i> | 18791955 | 596 | 94% | 60.8% |

Table 3 Proportion of errors for the various schemes used in ATCMPSK.

Error roof = 0.01, interleaving size = 32*16, SNR=24 dB.

The results given in Table 3 are for ATCMPSK with no interleaving and an error roof of 0.01 with SNR = 24 dB. There are two important points illustrated by this table. First of all, 0.3% of total transmissions are carried out using schemes better than TCQPSK. This may appear as a small number, but if those transmission had been performed using TCQPSK, and if they had all been in error, then the probability of error would have increased by 0.003. Of course, not all these symbols are in error when TCQPSK is employed. This—and the fact that higher rate codes with worse BER are used—is why the difference between the two schemes at that SNR is about 0.00025 (see Figure 27).

One other important point is that although the low rate repetition schemes are used seldom, their contribution to BER is significant. To explain this we must realize that these schemes occur during very deep fades and that is why they contribute so much to the overall BER.

The comparison made between ATCMPSK and TCQPSK is only valid at relatively low values of SNR where the throughput of the adaptive scheme is comparable to that of

the fixed rate code. At high SNR, where the throughput of ATCMPSK is considerably larger than one we can compare the scheme with the rate 2/3 pragmatic TC8PSK scheme, as given in Figure 28.

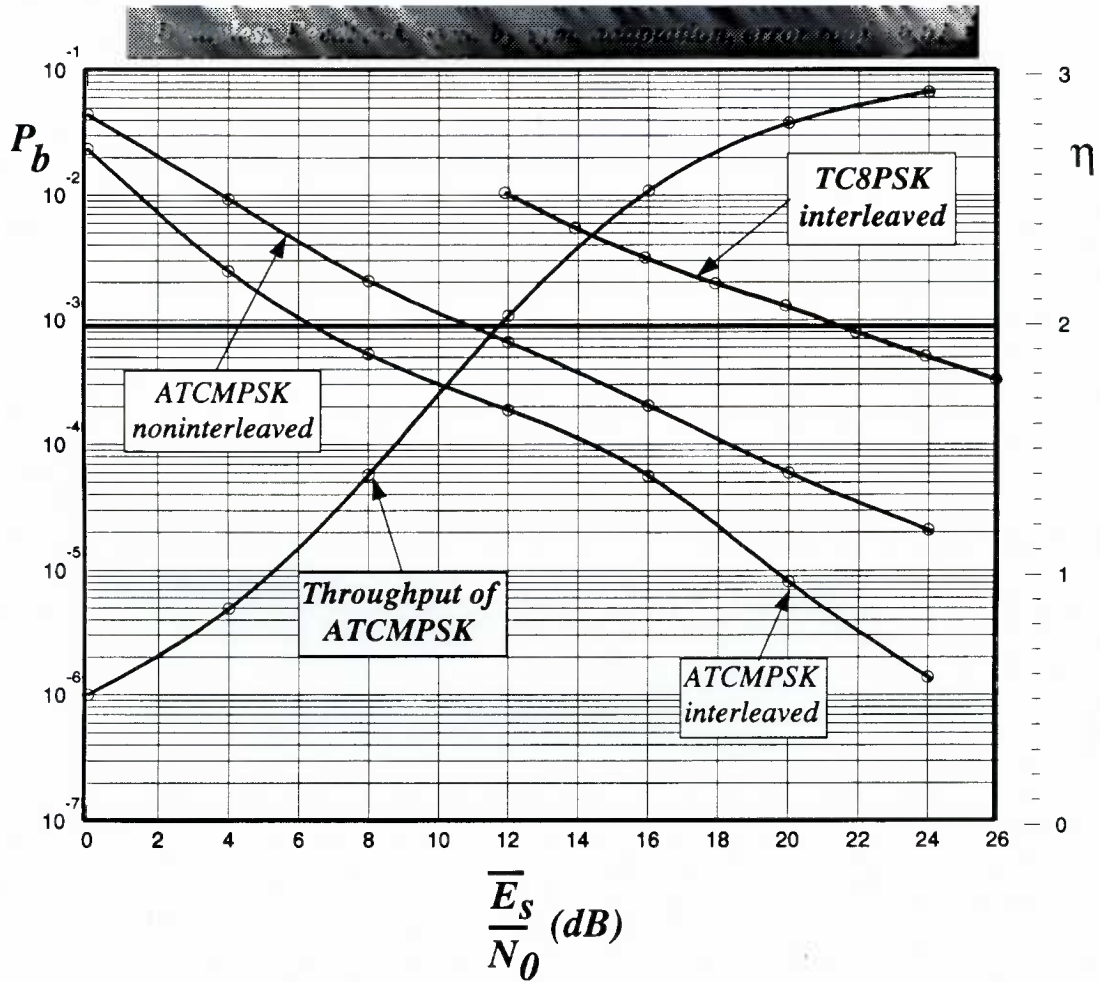


Figure 28 BER curves for ATCMPSK and fixed rate TC8PSK, with superimposed curve of the throughput performance of ATCMPSK.

The throughput of the ATCMPSK scheme is 2 which is the throughput of TC8PSK scheme at SNR = 12dB. The BER for ATCMPSK at 12 dB is 2×10^{-4} while for TC8PSK it is 10^{-2} which is 50 times as large. Therefore we get an improvement of almost two orders

of magnitude. In terms of dB gain, we can observe—by interpolation—that TC8PSK has the same BER (as ATCMPSK at 12 dB) at SNR=28 dB which translates to 16 dB gain.

Moreover, to achieve a throughput of 3 using a fixed rate code we need to use a scheme such as TC16PSK. The gain obtained by applying the adaptive scheme is even greater in this case (see Figure 19). We can therefore conclude that a **substantial gain** on the order of 3 – 20 dB is obtained using ATCMPSK with the error roof of 0.01. Using different thresholds, we can further improve the BER performance at the expense of a reduction in throughput.

7.4.4 Effect of Vehicle Speed or B_dT_s Product

Since we are considering only the effect of fading amplitude on the transmitted signal, we should expect that increasing the speed of the vehicle—and hence the B_dT_s product—would only correspond to less correlated adjacent signals. That is, as the speed of the vehicle increases, the fading process becomes faster, and attenuated signals become less and less correlated. Therefore, we would expect that the performance of the system will improve with increasing speed. In fact, the limiting case for this improvement is the case of ideally interleaved scheme in which there is no correlation between adjacent signals. Figure 29 shows the performance curves for the adaptive scheme for different vehicle speeds.

One must be aware, however, that, in most practical applications using noncoherent and differential detection schemes, the BER performance becomes progressively worse with increasing speed. The degradation in performance is reflected through error floors which occur at higher error probabilities for higher speeds.

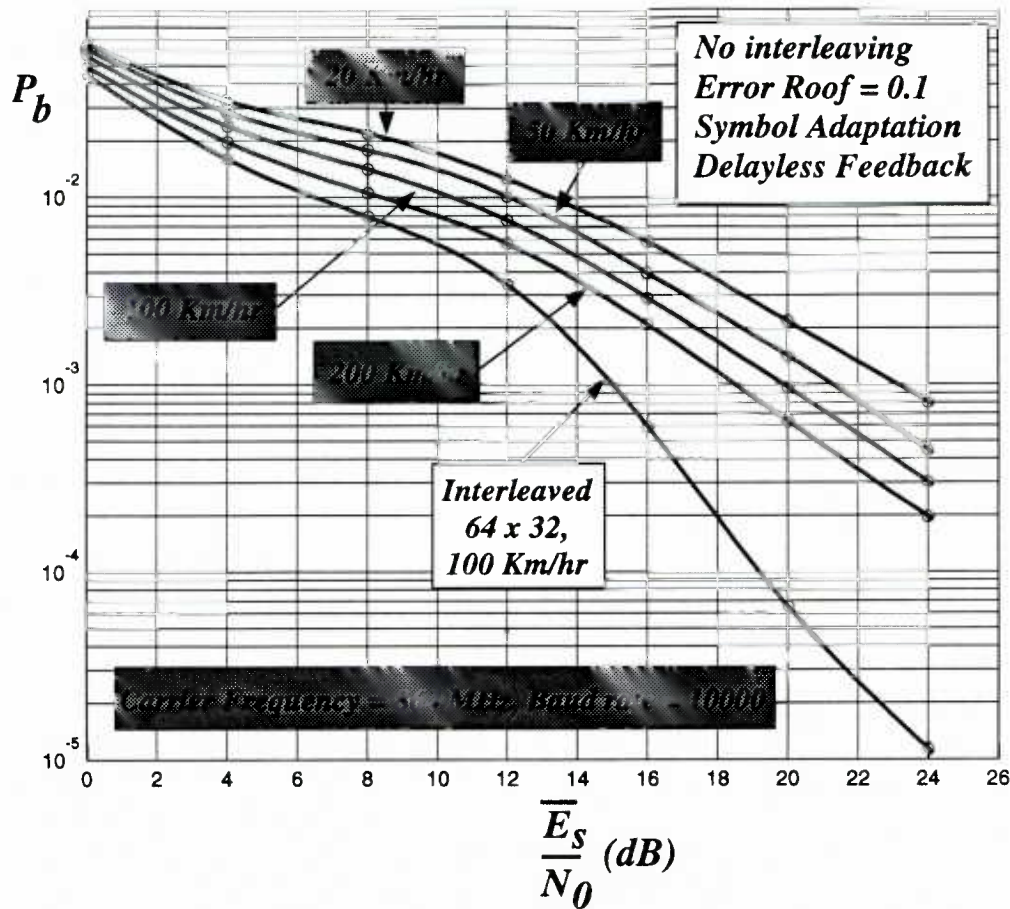


Figure 29 Effect of vehicle speed on the BER performance of ATCMPSK with delayless feedback.

Furthermore, if there is delay in the feedback channel, increasing the speed will make CSI less accurate to the point that eventually increasing the speed will result in degradation of performance. The effect of speed on the ATCMPSK scheme with a feedback delay equivalent to one symbol duration (0.1 msec for a Baud rate of 10000) is shown in Figure 30.

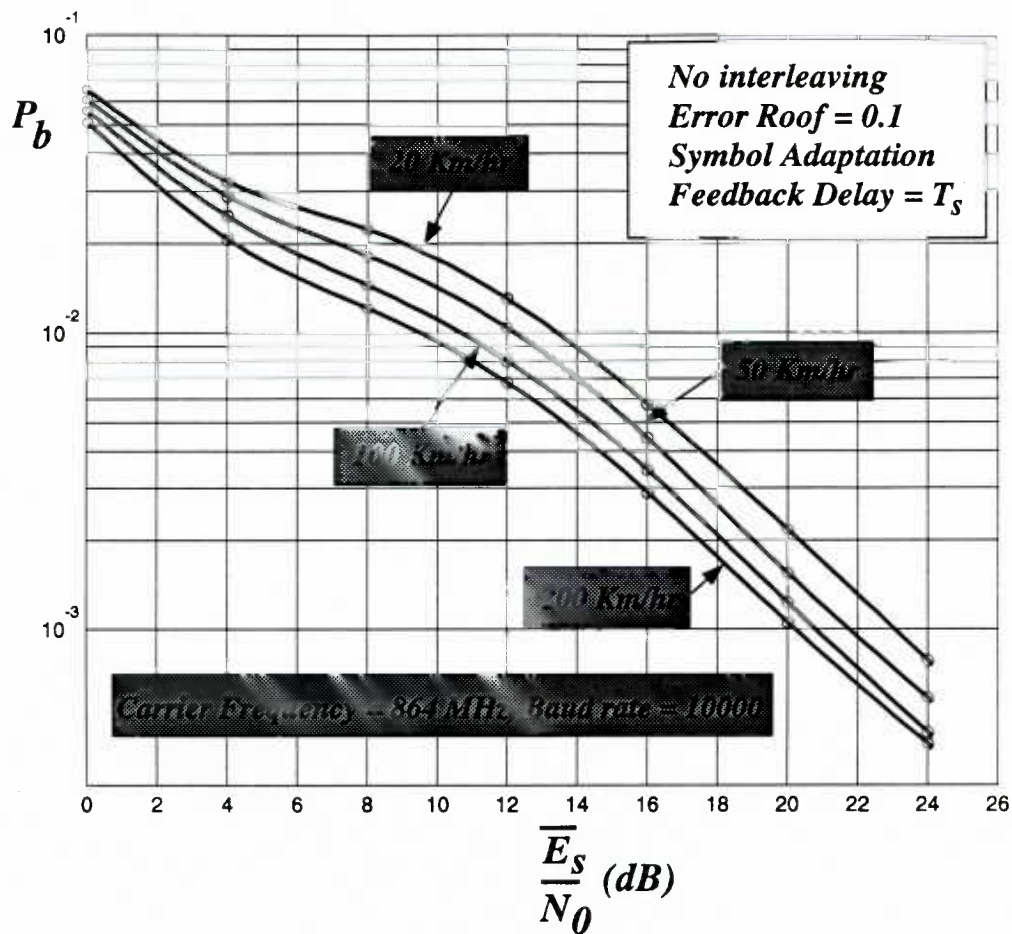


Figure 30 Effect of vehicle speed on the BER performance of ATCMPSK, feedback delay = 1 symbol duration.

The BER performance of a faster moving mobile is still better, but the improvement in performance due to less correlation in adjacent symbols has become less significant. If the feedback delay is increased to three symbol durations, then the picture changes greatly. The performance gets progressively worse as the speed of the mobile increases. Figure 31 depicts this phenomenon.

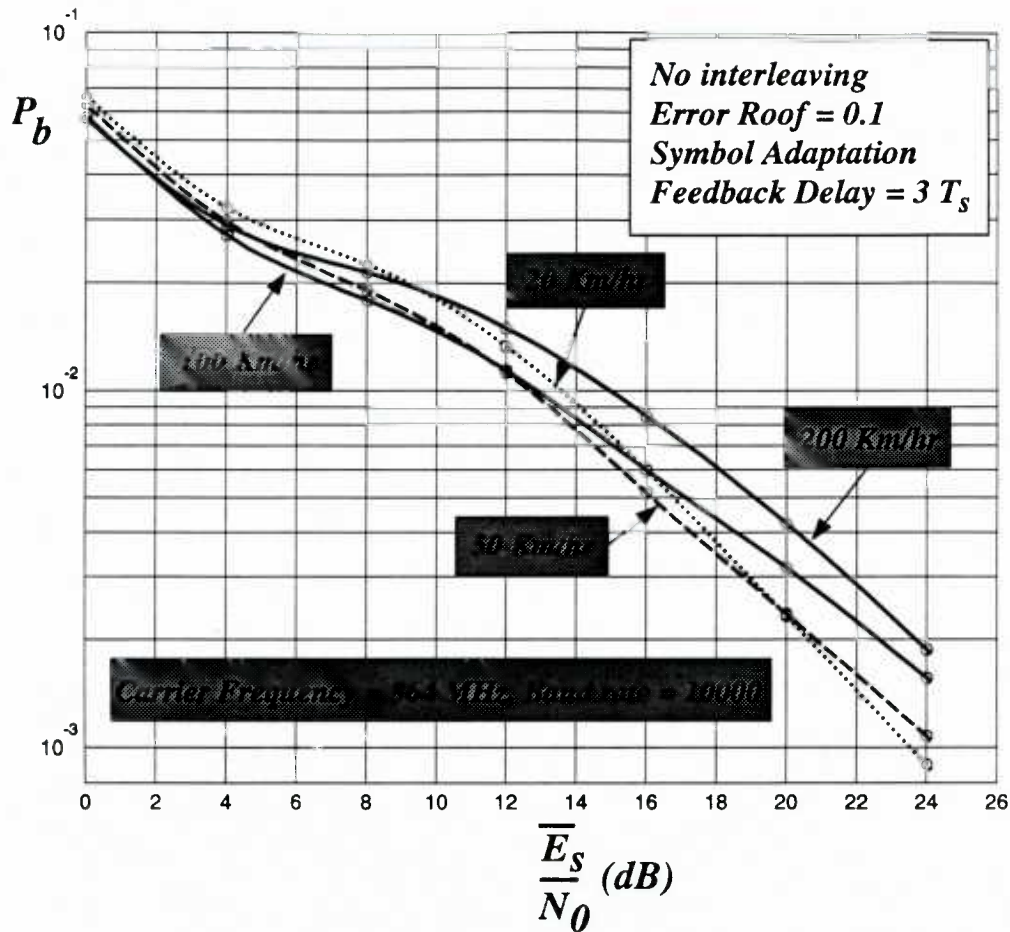


Figure 31 Effect of vehicle speed on the BER performance of ATCMPSK, feedback delay = 3 symbol durations.

As the speed of the vehicle increases, CSI becomes less and less accurate; that is, the delay in the feedback channel translates into a greater change in channel conditions. Therefore, the BER performance degrades with increasing speed.

7.4.5 Effect of Feedback Delay and Adaptation Interval

In practice, it is very difficult to achieve delayless feedback. In order to take into account the effect of delay, we will assume that delay τ is constant, and therefore the receiver is aware of the behaviour of the transmitter at any signalling instant. That is, the receiver knows exactly what modulation scheme has been used by the transmitter.

In order to observe the effect of feedback delay, a vehicle speed of 100 km/hr and feedback delays equivalent to up to five symbol duration are considered; that is the range $B_d\tau \approx 0.01...0.04$. Figure 32 shows how the performance of the scheme deteriorates with increasing feedback delay.

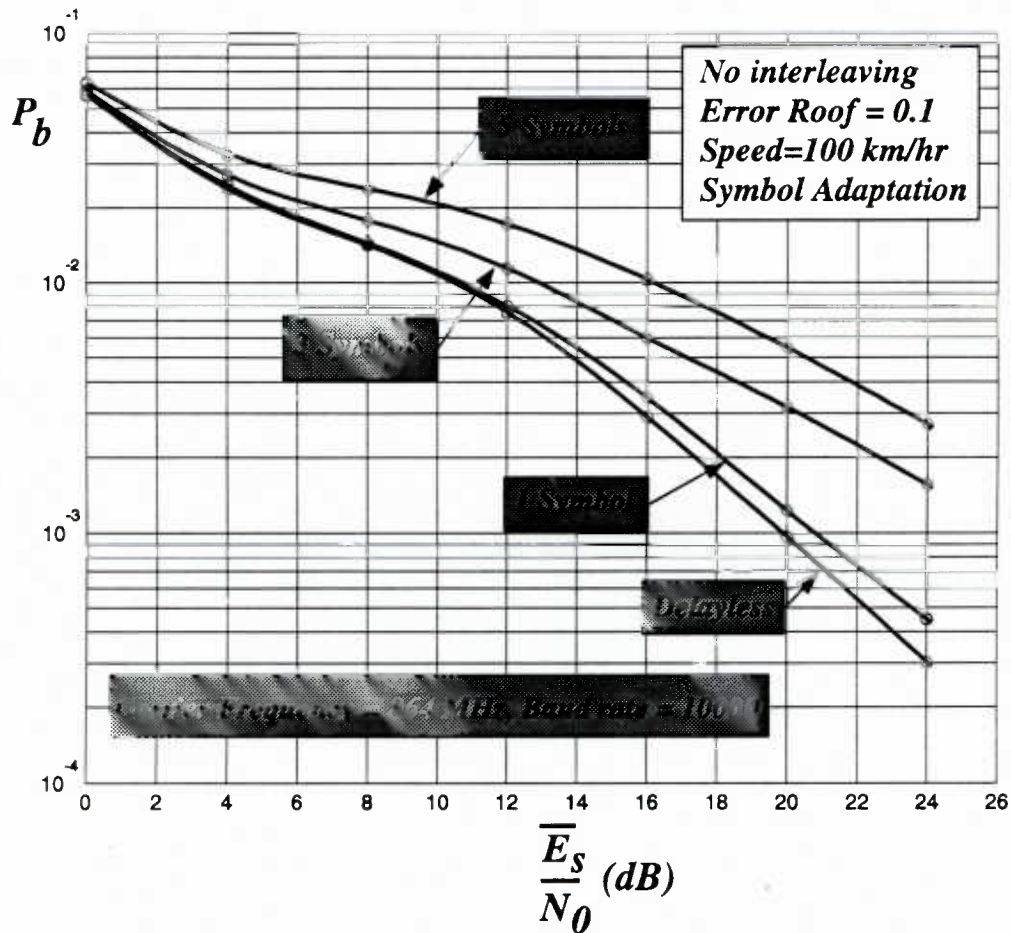


Figure 32 Effect of feedback delay on the BER performance of ATCMPSK.

A small feedback delay—much smaller than the maximum duration of fades—does not amount to a considerable change in performance. However, when the delay becomes large—as for the case of 3 symbol durations in Figure 32—the degradation in performance

becomes very significant. This is due to the fact that CSI becomes more outdated as the delay in the feedback channel increases.

All the simulations so far have assumed ideal (symbol-by-symbol) adaptation. The effect of adapting the modulation rate to channel conditions at fixed intervals greater than 1 symbol duration is given in Figure 33.

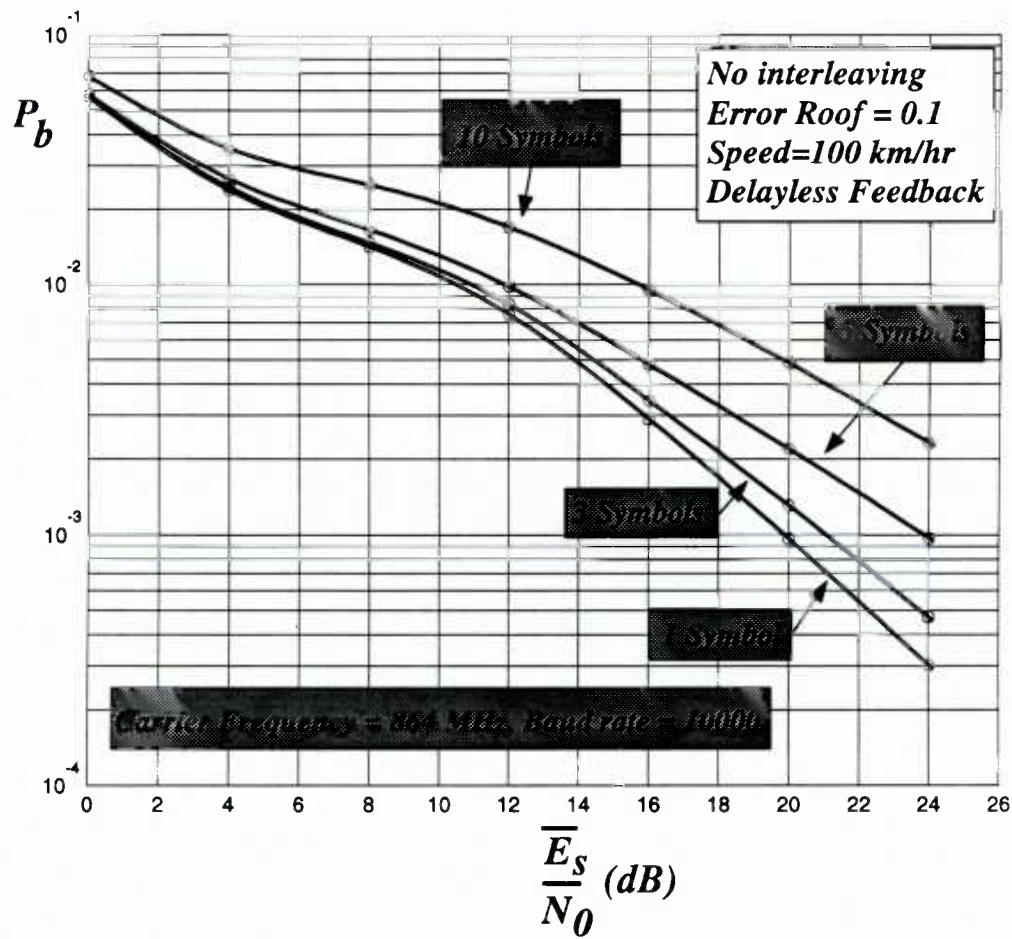


Figure 33 Effect of nonideal adaptation on the BER performance of ATCMPSK.

As expected, the BER performance degrades progressively as the duration of the adaptation interval is increased. This is again due to the fact that channel conditions at the start of an adaptation interval may change significantly before the next interval has

been started. Moreover, the effect of the adaptation interval is of course a function of the fading process. For fast fading, a few symbol durations may result in considerable change in channel conditions, and therefore an adaptation interval of such length will degrade the performance significantly. However, for very slow fading we may be able to get away with a few symbol duration between two adaptation instants without paying a big price in performance. Symbol-by-symbol adaptation is of course ideal for every application. But, it may not be practically feasible in which case the length of the adaptation interval should be chosen to keep the BER at a tolerable level.

Chapter 8

Conclusions and Recommendations for Future Research

Although fixed rate trellis codes are comparably good in terms of error performance in Rayleigh fading channels, they fail to explore the time varying nature of these channels, and are often designed conservatively to combat very poor channel conditions. The fixed rate of transmission hence results in sacrificing the effective information rate during good channel conditions.

We have proposed an adaptive trellis-coded scheme called ATCMPSK which explores the time varying nature of Rayleigh fading channels, and is extremely effective in combating fading. The ATCMPSK scheme is pragmatic in terms of its design and implementation. The most complicated component of our system (regarding the coding and the modulation aspects of the design) is a rate 1/2 convolutional encoder, and a Viterbi decoder that is capable of constructing parallel branches in its state transitions, uses the Gaussian metric for decoding, and treats repeated symbols on a single transition in the trellis diagram. We have suggested a mapping scheme called double-Gray-coded mapping which results in better performance for MPSK signals with $M=16$ or larger, as compared to sectorized-Gray-coded mapping.

Since the conventional deterministic approach to interleaving/deinterleaving does not suit the adaptive scheme, an alternative method to remove the memory in the channel has been introduced. It has been shown that there is lot to be gained from interleaving specially at high SNR values where the high rate schemes are prevalent.

The ATCMPSK scheme results in 3–20 dB gain in BER performance, as compared to fixed rate codes. These gains have been obtained using a simple encoder of constraint length three, under ideal conditions. We have investigated the loss in performance due to nonideal conditions, and shown that even under nonideal conditions one achieves a very substantial gain using the adaptive scheme.

We have suggested that one way of determining the adaptation intervals is to use the BER performance curves (in the AWGN channel) of the individual schemes used in ATCMPSK, and set the threshold in such a way as to keep BER below a certain level. However, there are many other ways in which the threshold can be chosen, and we can in fact shape the BER curves, within the performance constraints of the scheme, by choosing different sets of thresholds.

We have used the conventional transfer function approach to find an upper bound for the BER performance, and used the statistics of the Rayleigh fading channel to formulate an almost exact expression for the throughput. Our theoretical results were consistent in terms of their agreement with simulations. By way of simulations, we showed the effects of some of the nonideal conditions, such as the delay in the feedback channel, and adaptation intervals larger than one symbol duration.

For future research, we suggest the following:

- Study a more realistic and practical model which takes into account the effect of multipath fading on the phase of the transmitted signals, and addresses the carrier phase tracking issue for the adaptive system. Implement the proposed scheme taking into account all the practical implications and issues involved in the design of the scheme.

- For the more realistic model, consider a system for which CSI consists of both the attenuation and the phase of the fading process.
- Consider prediction-adaptation techniques to reduce the transmission rate of CSI in the feedback channel.
- Study the implementation of the system with differential detection schemes such as *multiple-symbol differential detection* suggested in [13].
- For practical channels, there are many considerations such as geography, ambient and climate which can change the characteristics of the channel. Study the application of learning systems and fuzzy logic to the adaptation process to optimize the performance of the scheme for specific channel considerations.
- Study effective methods of monitoring the channel conditions, and providing CSI to the transmitter in the most efficient manner.

Bibliography

- [1] Guest Editor: W. Y. C. Lee, "Invited special issue papers on digital cellular technologies," *IEEE Transactions on Vehicular Technology*, vol. 40, pp. 291–375, May 1991.
- [2] G. Ungerboeck, "Channel coding with multilevel/phase signals," *IEEE Transactions on Communications*, vol. IT-28, pp. 55–67, January 1982.
- [3] J. K. Cavers, "Variable-rate transmission for Rayleigh fading channels," *IEEE Transactions on Communications*, vol. COM-20, pp. 15–22, Feb. 1972.
- [4] A. J. Viterbi, J. K. Wolf, E. Zehavi, and R. Padovani, "A pragmatic approach to trellis-coded modulation," *IEEE Communications Magazine*, pp. 11–19, July 1989.
- [5] G. Ungerboeck, "Trellis-coded modulation with redundant signal sets. Part I: Introduction; Part II: State of the art," *IEEE communications Magazine*, vol. 25, pp. 5–21, February 1987.
- [6] J. F. Hayes, "Adaptive feedback communications," *IEEE Transactions on Communications*, vol. COM-16, pp. 29–34, Feb. 1968.
- [7] V. O. Hentinen, "Error performance for adaptive transmission on fading channels," *IEEE Transactions on Communications*, vol. COM-22, pp. 1331–1337, Sept. 1974.
- [8] W. Jakes, *Microwave mobile communications*, ch. 1. New York: Wiley, 1974.
- [9] M. K. Simon, "Dual pilot tone calibration technique (DTCT)," *IEEE Transaction on Vehicular Technology*, vol. VT-35, pp. 63–70, May 1986.
- [10] F. Davarian, "Mobile digital communications via tone calibration," *IEEE Transactions on Vehicular Technology*, vol. VT-36, pp. 55–62, May 1987.
- [11] F. M. Gardner, *Phaselock techniques*, ch. 9. Wiley-interscience, 2 ed., 1979.
- [12] D. Makrakis and P. T. Mathiopoulos, "Optimal decoding in fading channels: a combined envelope, multiple differential and coherent detection approach," *Proceedings of GLOBECOM '89, Dallas, Texas*, pp. 1551–1557, November 1989.

- [13] D. Divsalar and M. K. Simon, "Multiple symbol differential detection of MPSK," *IEEE Transactions on Communications*, vol. 38, pp. 300–308, March 1990.
- [14] R. E. Blahut, *Digital transmission of information*, ch. 11, pp. 444–445. Addison Wesley, 1990.
- [15] J. Hagenauer, "Viterbi decoding of convolutional codes for fading–And burst channels," *1980 Int. Zurich Seminar on Digital Communications*, pp. G2.1–G2.7, March 1980.
- [16] S. Kallel, "Analysis of a type II, hybrid, ARQ Scheme with code combining," *IEEE Transactions on Communications*, vol. 38, pp. 1133–1137, August 1990.
- [17] S. Lin and J. D. J. Costello, *Error control coding: fundamentals and applications*, ch. 14. Prentice-Hall, 1983.
- [18] A. J. Viterbi and J. K. Omura, *Principles of digital communication and coding*, ch. 3. McGraw-Hill, New York, 1979.
- [19] E. Biglieri and D. Divsalar and P. J. McLane and M. K. Simon, *Introduction to trellis-coded modulation with applications*, ch. 4. MacMillan, 1991.
- [20] M. M. Mulligan and S. G. Wilson, "An improved algorithm for evaluating trellis phase codes," *IEEE Transactions on Information Theory*, vol. IT-30, pp. 846–851, November 1984.
- [21] R. C. P. Saxena, "Optimum encoding in finite state coded modulation," Tech. Rep. TR83-2, Department of Electrical, Computer and System Engineering, Rensselaer Polytechnic Institute, Troy, N.Y., 1983.
- [22] E. Zehavi and J. K. Wolf, "On the performance evaluation of trellis codes," *IEEE Transactions on Information Theory*, vol. IT-33, pp. 196–201, March 1987.
- [23] W. H. Press, B. P. Flannery, A. Teukolsky, and W. T. Vetterling, *Numerical recipes in C*, ch. 7. Cambridge, 1988.

Appendix A The Gaussian Metric

To prove that the Gaussian metric is a maximum likelihood metric for Rayleigh fading channels with ideal CSI, we can use a model as shown in Figure 34. A matched filter receiver decides what signal has been transmitted.

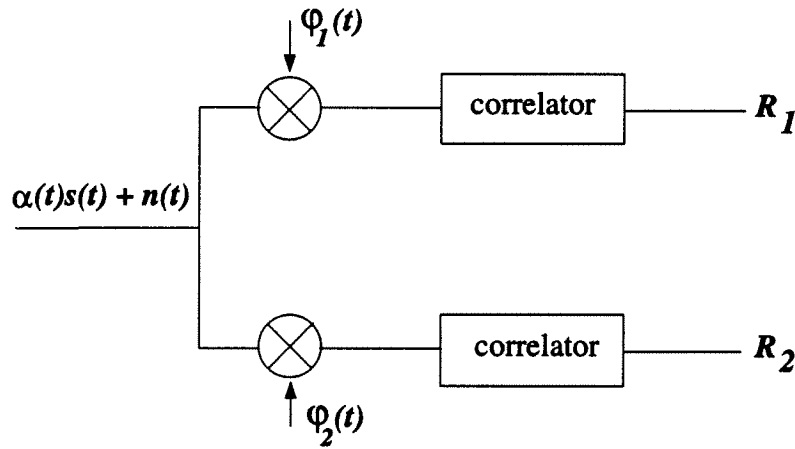


Figure 34 Correlator receiver for maximum likelihood detection.

The transmitted signal $s(t)$ is attenuated by the time varying amplitude of fading $\alpha(t)$, and corrupted by AWGN $n(t)$. $\phi_1(t)$ and $\phi_2(t)$ are the following orthonormal functions:

$$\begin{aligned}\varphi_1(t) &= \sqrt{\frac{2}{T}} \cos(2\pi f_c t) \\ \varphi_2(t) &= \sqrt{\frac{2}{T}} \sin(2\pi f_c t).\end{aligned}\tag{A.1}$$

The signals in the signal space can then be expressed as:

$$s_i(t) = s_{i1}\varphi_1(t) + s_{i2}\varphi_2(t).\tag{A.2}$$

The output of the correlator is the received signal:

$$\begin{aligned}
 R_i &= \int_0^T r(t)\phi_i(t) dt \\
 &= \int_0^T (\alpha(t)s(t) + n(t)) dt.
 \end{aligned}
 \tag{A.3}$$

The probability density function of the received signal given signal s_i was transmitted is:

$$\begin{aligned}
 R_1 | s_i &= \int_0^T \alpha(t)s_i(t)\phi_1(t) dt + \overbrace{\int_0^T n(t)\phi_1(t) dt}^{N_1} \\
 &= \int_0^T \alpha(t)(s_{i1}\phi_1(t) + s_{i2}\phi_2(t)) dt + N_1.
 \end{aligned}
 \tag{A.4}$$

Assuming that $\alpha(t)$ is constant for the duration of symbol $[0, T]$, we have:

$$\begin{aligned}
 R_1 | s_i &= \alpha \int_0^T s_{i1}\phi_1(t)\phi_1(t) dt + \int_0^T s_{i2}\phi_1(t)\phi_2(t) dt + N_1 \\
 &= \alpha s_{i1} + N_1
 \end{aligned}
 \tag{A.5}$$

where the second integral is zero since $\phi_1(t)$ and $\phi_2(t)$ are orthonormal functions. We can conclude that:

$$\begin{aligned}
 E[R_1 | s_i] &= \alpha s_{i1} + E[N_1] \\
 &= \alpha s_{i1}
 \end{aligned}
 \tag{A.6}$$

The same argument holds for $R_2 | s_i$.

The variance of the random variable:

$$\begin{aligned}
\text{var}[R_1 | s_i] &= E \left[\{(R_1 | s_i) - E(R_1 | s_i)\}^2 \right] \\
&= E \left[\{(\alpha s_{i1} + N_1) - \alpha s_{i1}\}^2 \right] \\
&= E[N_1^2] = \frac{N_0}{2}.
\end{aligned} \tag{A.7}$$

In conclusion:

$$R_j | s_i \sim N(\alpha s_{ij}, N_0/2), \tag{A.8}$$

or equivalently

$$f_{R_j | s_i} = \frac{1}{\sqrt{\pi N_0}} \exp \left(-(r_j - \alpha s_{ij})^2 / N_0 \right). \tag{A.9}$$

To prove that R_1 , R_2 are uncorrelated, note that:

$$\begin{aligned}
E[\{R_1 - E[R_1]\}\{R_2 - E[R_2]\}] &= E[\{\alpha s_{i1} + N_1 - \alpha s_{i1}\}\{\alpha s_{i2} + N_2 - \alpha s_{i2}\}] \\
&= E[N_1 N_2] = 0.
\end{aligned} \tag{A.10}$$

Now, since R_1 , R_2 are independent and uncorrelated, we can state that:

$$\begin{aligned}
f_{\underline{R} | s_i}(r_1, r_2) &= f_{R_1 | s_i}(r_1) f_{R_2 | s_i}(r_2) \\
&= \frac{1}{(\sqrt{\pi N_0})^2} \exp \left(-(r_1 - \alpha s_{i1})^2 / N_0 \right) \exp \left(-(r_2 - \alpha s_{i2})^2 / N_0 \right) \\
&= \frac{1}{\pi N_0} \exp \left(- \left[(r_1 - \alpha s_{i1})^2 + (r_2 - \alpha s_{i2})^2 \right] / N_0 \right).
\end{aligned} \tag{A.11}$$

The optimum decision rule for maximum likelihood is to choose signal s_k iff:

$$f_{\underline{R} | s_k}(r_1, r_2) > f_{\underline{R} | s_i}(r_1, r_2) \quad \forall i \neq k, \tag{A.12}$$

or equivalently:

$$\left[(r_1 - \alpha s_{k1})^2 + (r_2 - \alpha s_{k2})^2 \right] < \left[(r_1 - \alpha s_{i1})^2 + (r_2 - \alpha s_{i2})^2 \right] \quad \forall i \neq k. \quad (\text{A.13})$$

For a sequence of length L of transmitted signals, the optimum decision is therefore:

Choose S_k iff :

$$\sum_{j=1}^L \left[(r_1 - \alpha_j s_{k1})^2 + (r_2 - \alpha_j s_{k2})^2 \right] < \sum_{j=1}^L \left[(r_1 - \alpha_j s_{i1})^2 + (r_2 - \alpha_j s_{i2})^2 \right]$$

QED. $\forall i \neq k$
(A.14)

Appendix B Comparison of Double-Gray-Coded Mapping and Sectorized-Gray-Coded Mapping

Sectorized-Gray-coded signal space for an MPSK signalling scheme has $M/4$ sectors. The first $\log_2(M) - 2$ bits in the encoded symbol choose one of those sectors lexicographically. In double-Gray-coded scheme, however, the sectors are also chosen according to Gray code. This concept is shown in Figure 5.

B.1 Comparison in AWGN

The effect of Gray coding of the sectors on the signals in the parallel branches of the signal space is shown in Figure 35.

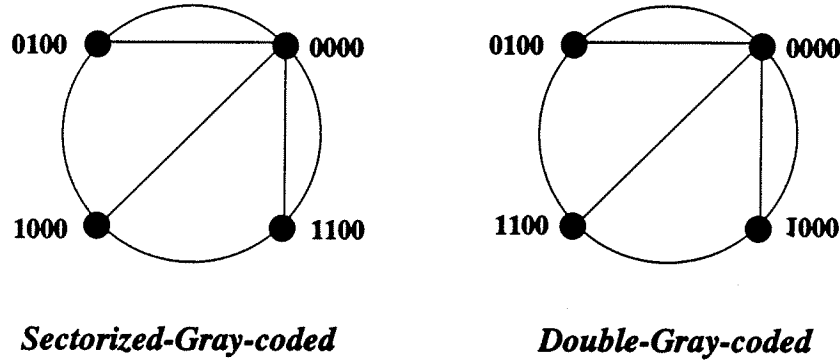


Figure 35 Comparison of signals on the parallel branches of the trellis diagram for double-Gray-coded and sectorized-Gray-coded mappings.

The two neighbouring signal differ in one bit, as compared to two for sectorized-Gray-coded mapping. For TC16PSK with sectorized-Gray-coded mapping, the probability of error due to parallel transitions is:

$$\begin{aligned}
 P_{\parallel} &= \frac{1}{3}p(1-p) + \frac{1}{3}p^2 + \frac{2}{3}p(1-p) \\
 &= p - \frac{2}{3}p^2 \approx Q\left(\sqrt{\frac{E_s}{N_0}}\right).
 \end{aligned}
 \tag{B.1}$$

This is approximately 2/3 of the same probability using sectorized-Gray-coded scheme indicated in 5.38. The expression for the overall probability of error is therefore:

$$P_b \leq p + Q\left(\sqrt{\frac{1.324E_s}{2N_0}}\right) e^{-\frac{1.324E_s}{4N_0}} \times \frac{1}{3} \frac{\partial T(D, I)}{\partial I} \Big|_{I=1; D=\exp\left(-\frac{E_s}{4N_0}\right)}. \quad (\text{B.2})$$

The error weight profile of the code is given in Table 4. Note that the first 7 elements in the Table are identical to those for the sectorized-Gray-coded mapping scheme. The second term in B.2—lets call it the *trellis error*—was found using the entries in Table 4, and the error-state diagram's set of branch labels given in (5.31).

| Error Pattern (e_i) | Error Weight Profile $W(e_i)$ |
|-------------------------|---|
| 0000 | 1 |
| 0001 | $D^{d_1^2}$ |
| 0010 | $\frac{D^{d_1^2} + D^{d_3^2}}{2}$ |
| 0011 | $D^{d_2^2}$ |
| 0100 | $D^{d_4^2}$ |
| 0101 | $\frac{D^{d_3^2} + D^{d_5^2}}{2}$ |
| 0110 | $\frac{D^{d_1^2} + D^{d_3^2} + D^{d_5^2} + D^{d_7^2}}{4}$ |
| 0111 | $\frac{D^{d_2^2} + D^{d_6^2}}{2}$ |
| 1000 | $D^{d_8^2}$ |
| 1001 | $D^{d_7^2}$ |
| 1010 | $D^{d_5^2}$ |
| 1011 | $D^{d_6^2}$ |
| 1100 | $D^{d_4^2}$ |
| 1101 | $\frac{D^{d_3^2} + D^{d_5^2}}{2}$ |
| 1110 | $\frac{D^{d_1^2} + D^{d_3^2} + D^{d_5^2} + D^{d_7^2}}{4}$ |
| 1111 | $\frac{D^{d_2^2} + D^{d_6^2}}{2}$ |

Table 4 Error weight profile for the rate 3/4 TC16PSK pragmatic code with sectorized-Gray-coded mapping.

Note that d_{free} is the same as the code with double-Gray-coded mapping. However, the new mapping results in a better code that has a slightly better BER performance as depicted in Figure 36.

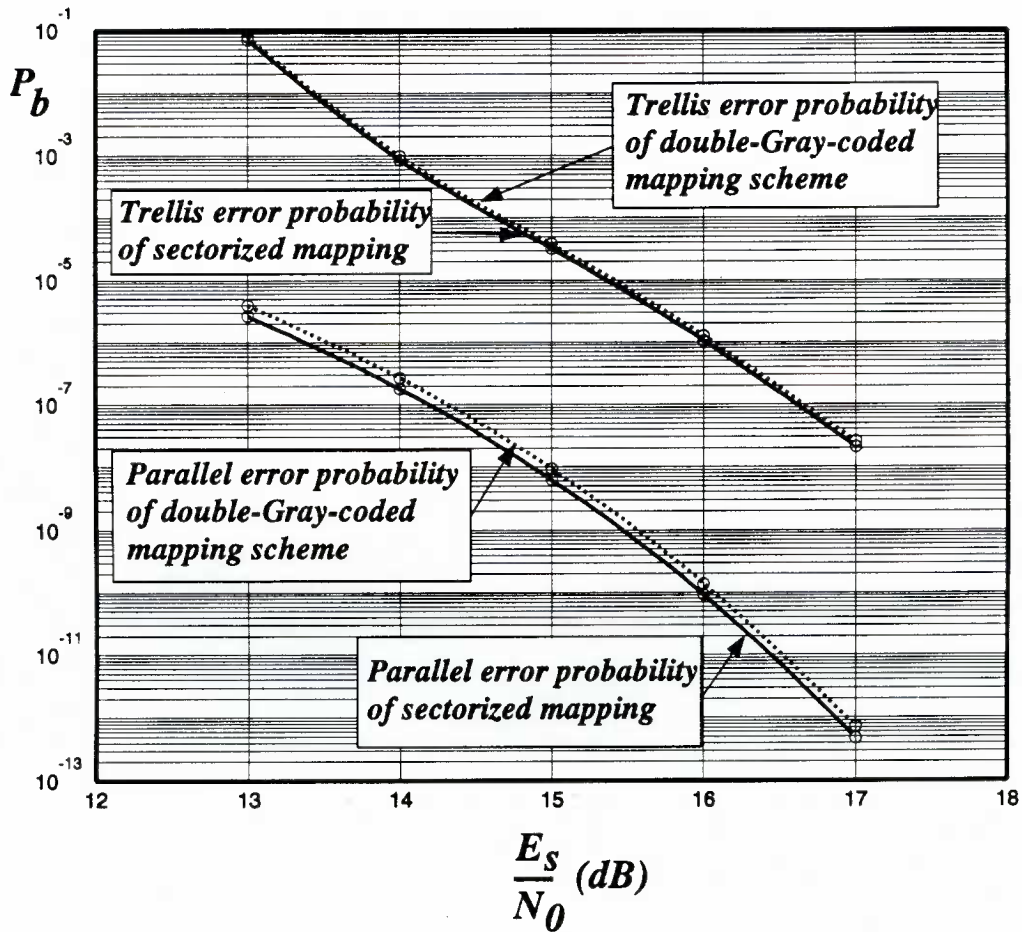


Figure 36 Comparison of trellis error and probability of error due to parallel transitions for TC16PSK in AWGN with sectorized-Gray-coded and double-Gray-coded mapping.

B.2 Comparison in Rayleigh Fading Channel

It was observed in the last section that the new mapping scheme does not result in a considerable improvement in BER performance in AWGN. However, in the Rayleigh fading channel, the probability of bit-error due to parallel transitions becomes the

dominating factor. Parallel branches do not have the opportunity to recover from deep fades. Therefore, one would anticipate that an improvement in the structure of the signals in parallel branches would have a relatively considerable effect on the BER performance.

Integrating B.1 over the Rayleigh fading density function, $P_{||}$ for the double-Gray-coded TC16PSK scheme is found to be:

$$P_{||} = \frac{1}{3} \sqrt{\frac{E_s/N_0}{2 + E_s/N_0}}. \quad (\text{B.3})$$

We can observe, that the first term is 2/3 of that of the scheme using sectorized Gray-coded mapping. The performance of rate 3/4 TC16PSK for both mapping schemes are given in Figure 37.

The asymptotic gain of the new mapping scheme for TC16PSK in Rayleigh fading is therefore around 1 dB, and it is as easy to implement as the sectorized-Gray-coded mapping. For larger constellations, the gain obtained from the new mapping is even more significant. For example, it is simple to show that for 32PSK the asymptotic BER with double-Gray-coded mapping is approximately half that of the scheme using sectorized-Gray-coded mapping.

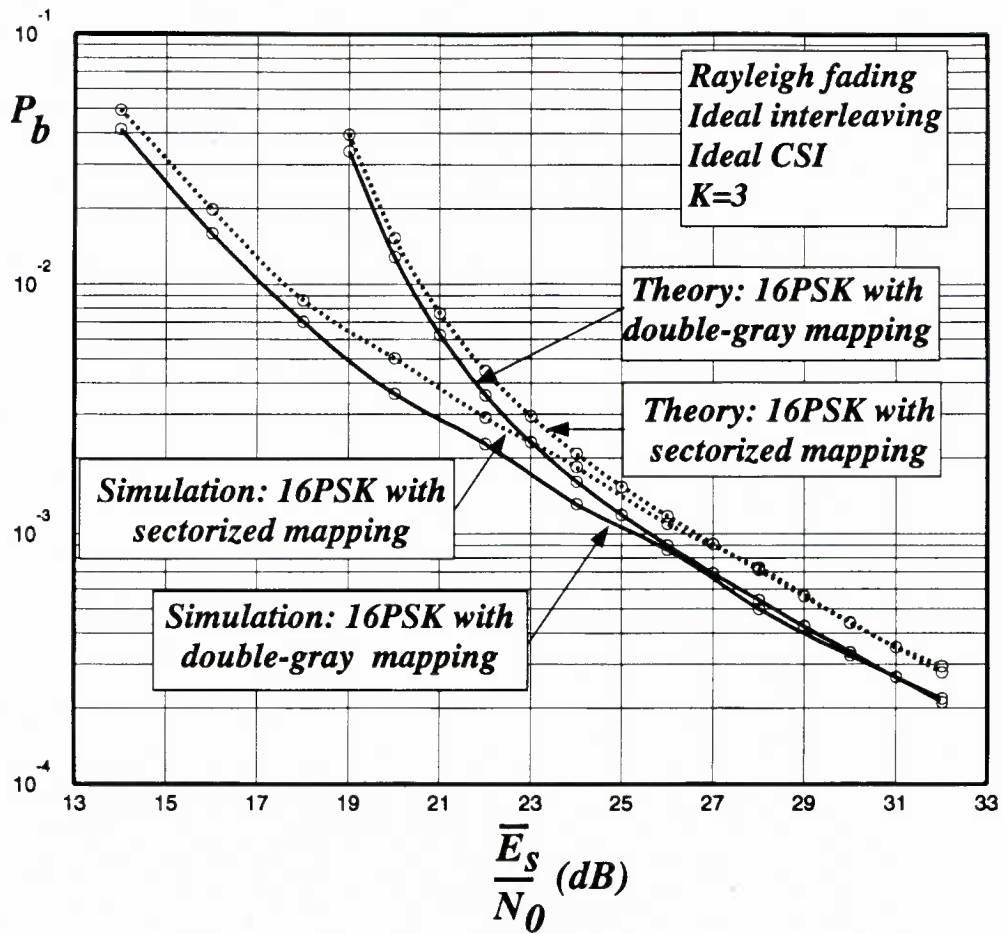


Figure 37 BER performance of double-Gray-coded TC16PSK.

Appendix C Confidence Interval for Simulation Results

The minimum number of the error events counted for the simulation results presented in this thesis was 200. However, for the case of ATCMPSK with ideal interleaving, and an error roof of 0.01 (see Figure 27) it would have taken about a week of computing time to obtain so many error events for SNR=24 dB (using a SPARC station 2). The actual number of error events was 58 in this case. To give an indication of how the number of error events reflect the accuracy of the simulation results, that particular point in the performance curve was run 5 times and the 95% confidence interval was calculated to be:

$$P_e(24 \text{ dB}) = 1.39 \times 10^{-6} \pm 0.25 \times 10^{-6}. \quad (\text{C.1})$$

The worst point for the case of noninterleaved ATCMPSK with an error roof of 0.1, at SNR = 24 dB was run for more than 1500 error events. The 95% confidence interval for this point is:

$$P_e(24 \text{ dB}) = 3.03 \times 10^{-4} \pm 0.07 \times 10^{-4}. \quad (\text{C.2})$$

The simulation points for lower values of SNR correspond to greater numbers of error events. Therefore, the confidence interval for these points is smaller, and they are hence more accurate.

BIOGRAPHICAL INFORMATION

NAME: Siavash Massoumi Alamouti

MAILING ADDRESS:

115 West 12th Ave.,
Vancouver, B.C. V5Y-1T6

PLACE AND DATE OF BIRTH: TEHRAN - IRAN

MARCH 16, 1962

EDUCATION (Colleges and Universities attended, dates, and degrees):

Cariboo college, Kamloops, B.C. 1984-1985

U.B.C.

1985-1989 B.A.Sc.

U.B.C.

1985-1991 M.A.Sc.

POSITIONS HELD:

PUBLICATIONS (if necessary, use a second sheet):

AWARDS:

B.C. Science Council GREAT award 1990
1991

Complete one biographical form for each copy of a thesis presented to the Special Collections Division, University Library.